nature biotechnology

Article

https://doi.org/10.1038/s41587-025-02854-y

Programmable promoter editing for precise control of transgene expression

Received: 10 July 2024

Accepted: 5 September 2025

Published online: 13 October 2025

Check for updates

Sneha R. Kabaria ®¹, Yunbeen Bae ®¹, Mary E. Ehmann ®¹, Brittany A. Lende-Dorn ®¹, Adam M. Beitz ®¹, Emma L. Peterman ®¹, Kasey S. Love ®², Deon S. Ploessl ®¹ & Kate E. Galloway ®¹⊠

Subtle changes in gene expression direct cells to distinct cellular states. Identifying and controlling dose-dependent transgenes require tools for precisely titrating expression. Here, we develop a highly modular, extensible framework called DIAL for building editable promoters that allow for fine-scale, heritable changes in transgene expression. Using DIAL, we increase expression by recombinase-mediated excision of spacers between the binding sites of a synthetic zinc finger transcription factor and the core promoter. By nesting varying numbers and lengths of spacers, DIAL generates a tunable range of unimodal setpoints from a single promoter. Through small-molecule control of transcription factors and recombinases, DIAL supports temporally defined, user-guided control of transgene expression that is extensible to additional transcription factors. Lentiviral delivery of DIAL generates multiple setpoints in primary cells and induced pluripotent stem cells. As promoter editing generates stable states, DIAL setpoints are heritable, facilitating mapping of transgene levels to phenotype and fate in direct conversion to induced motor neurons. The DIAL framework opens opportunities for tailoring transgene expression and improving the predictability and performance of gene circuits across diverse applications.

Over time, small changes in gene expression can generate diverging cell fates¹⁻⁶. Overexpression of endogenous and synthetic genes drives and redirects native processes and can augment native cellular functions⁷⁻¹⁰. However, identifying which transgenes elicit these subtle effects requires fine-tuned control, and implementing control over dosage-sensitive regimes remains a challenge^{1,11}. In particular, nonlinear effects of gene expression can confound inference of positive and negative regulation of phenotypes^{1,2,12,13}. Tools that support fine-scale titration of expression reveal nonmonotonic relationships between expression of regulators and phenotypes^{1,2,12}. While useful for identifying linear regulators, large-scale screening tools such as CRISPR-based knockout, knockdown and activation often do not provide sufficient resolution to find regulators with nonlinear relationships to phenotypes. Such CRISPR-based screening does not predict how overexpression of transgenes influences cellular behaviors¹⁴. As

transgenes are increasingly used to augment cellular functions and program cell fate, there is a critical need for scalable tools to identify regulators with complex functions and define their influence on physiologically relevant phenotypes $^{14-17}$.

Tools that support titration may also enable tuning and control of transgene expression in therapeutic contexts for precision cell and gene therapy 10 . To this end, synthetic biology aims to harness the power of native biology by interfacing native and synthetic gene regulatory networks. Dynamic synthetic circuits such as toggle switches, pulse generators, bandpass filters and oscillators can dynamically control transgenes to direct cellular processes, states and identities $^{18-25}$. However, rational de novo design of synthetic circuits remains challenging $^{26-30}$. Even simple inducible promoters can exhibit emergent, undesirable behaviors that impede the development of transgenic systems and gene circuits $^{31-33}$.

¹Department of Chemical Engineering, MIT, Cambridge, MA, USA. ²Department of Biological Engineering, MIT, Cambridge, MA, USA. 🖂 e-mail: katiegal@mit.edu

Synthetic transcription factor systems offer constitutive and inducible control of gene expression 10,12,34,35. Synthetic transcription factors mimic the DNA-binding and transcriptional activation of native factors by modularly fusing high-affinity DNA-binding domains to strong transactivation domains (TADs). These synthetic transcription factors are often directed to binding sites upstream of a weak core promoter³⁴⁻³⁶. Properties of transcription factor binding sitesincluding number, distance to the core promoter and affinity of binding-influence the recruitment of transcriptional machinery and thus the level of transgene expression^{35,37}. Within a limited range, increasing levels of synthetic transcription factors or small-molecule inducers can increase the mean level of expression across a population of cells³². However, these tools generally result in bimodal distributions of expression 33,35,38. Bimodality limits robust control of the entire population and may confound construction of a functional relationship between levels of expression and phenotypes. More complex circuits can linearize inducible systems to generate unimodal dose-responses at the cost of larger payloads and numbers of genetic parts, which may be difficult to translate to relevant cell types³⁹.

To develop DIAL, we outlined a set of desirable features for a promoter system that controls transgene expression over dosage-sensitive regimes from a single promoter. First, we want a system capable of generating tunable setpoints of transgene expression that span physiologically relevant ranges, supporting titration of transgene levels from a single promoter. Second, setpoints should be unimodal to ensure uniform induction and reliable control across an entire population of cells. Third, to ensure stable, homogenous output levels, setpoints should be robust to fluctuations in the levels of system components. Fourth, to map setpoint levels to phenotypes, setpoints should be recordable and heritable. Since phenotypes can emerge over longer timescales, an ideal synthetic promoter system generates stable setpoints via heritable changes that can be read at terminal timepoints. Fifth, to control induction, the system should be amenable to user-guided cues that implement reversible and irreversible changes in expression from a single promoter. Finally, for translational impact, the synthetic promoter system should be compact for delivery into primary cells.

Here we expand the precision and tunability of synthetic promoters by developing a system capable of generating multiple setpoints of transgene expression from a single promoter. Through a defined combination of inputs, the DIAL promoter system generates multiple unimodal setpoints via promoter editing (Fig. 1a). Recombinase-based editing of the DIAL promoter excises a spacer between the binding sites

and core promoter. Reducing the distance between the binding sites and core promoter increases transcriptional activity, shifting expression to a higher setpoint. Increasing the length of the spacer increases the setpoint range by reducing the expression from the pre-edited promoter. By nesting orthogonal recombinase sites, we constructed a nested DIAL promoter that generates four stable setpoints from a single promoter. Importantly, we demonstrate that DIAL setpoints are robust over a large range of transactivator levels. As promoter editing is genetically encoded, DIAL translates user-defined inputs into heritable setpoints. To further explore the generality of the spacer-excision architecture, we integrated the TET-On system into the DIAL framework, generating TET-DIAL. TET-DIAL generates doxycycline (DOX)-inducible setpoints, allowing compact, reversible control of setpoint induction. For broad translation to diverse cell types, we demonstrate that DIAL can be delivered using lentivirus and generates setpoints of transgene expression in primary cells and human induced pluripotent stem cells (iPSCs). By controlling expression of a cell-fate regulator, DIAL setpoints dictate the rate of cell-fate transitions.

Results

Promoter editing generates a range of unimodal setpoints from a single promoter

Native transcription factors commonly use Cys2-His2 zinc finger (ZF) binding domains to identify cognate binding sites across the genome^{40,41}. Synthetic ZF transcription factors are designed to bind arrays of unique binding sites orthogonal to native sequences^{34,35}. Zinc finger activators (ZFas) induce transcription by binding near core promoters via their ZF DNA-binding domain and recruiting transcriptional machinery via their TAD. To compose the DIAL promoter system, we turned to a set of well-defined ZFas from the COMET toolkit^{34,35}. We designed the DIAL promoter with an array of tessellated binding sites specific to two ZF domains (ZF43, ZF37) separated from a downstream YB_TATA minimal promoter by a spacer (Fig. 1b and Supplementary Fig. 1a,b). Between the minimal promoter and binding site array, we placed a spacer flanked by loxP ('floxed') recognition sites. The tyrosine recombinase Cre recognizes the loxP sites and edits the promoter by excising the floxed spacer. Spacer excision brings the binding site array closer to the minimal promoter. In the presence of the ZFa, Cre-mediated excision increases expression from a low to a high setpoint (Fig. 1b). In the absence of ZFa, expression is OFF. Using a combination of Cre and ZFa, we program three setpoints of gene expression from a single promoter sequence (Fig. 1c).

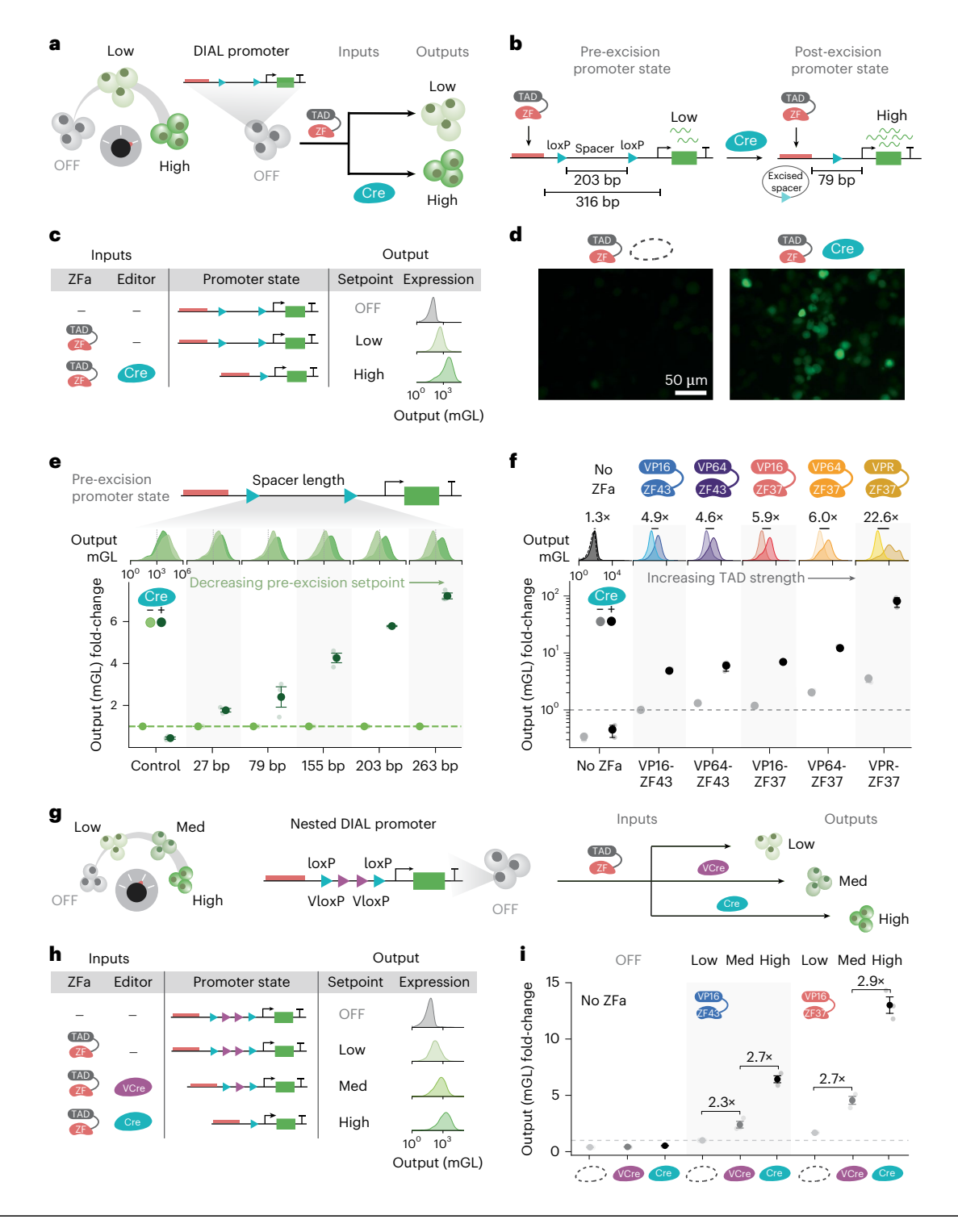
Fig. 1 | Promoter editing generates a range of unimodal setpoints from a single promoter. a, The DIAL promoter system uses combinatorial inputs of a synthetic ZF transcription factor with a TAD (ZFa) and Cre recombinase to generate distinct setpoints of gene expression from a single promoter. b, The pre-excision and post-excision states of the 203-bp DIAL promoter before and after Cre-mediated editing, respectively. The excision of the floxed 203-bp spacer increases expression by reducing the distance between the ZF binding sites and YB_TATA minimal promoter from 316 bp to 79 bp. c, Logic table of inputs, ZFa and Cre, and outputs, expected promoter state, target setpoint and observed gene (mGL) expression from the DIAL promoter. Output reporter mGL single-cell distributions from 203-bp DIAL promoter and different input combinations transfected on plasmids into HEK293T cells show output increase upon addition of ZFa (VP16-ZF37) and Cre. Different combinations of inputs enable three setpoints. d, Representative fluorescence microscopy images at 3 dpt of mGL expressed from 203-bp DIAL promoter transfected with ZFa (VP16-ZF37) on plasmids into HEK293T cells, with or without Cre (n = 3). Scale bar, 50 μm. e, Output reporter mGL geometric mean (gmean) fluorescence intensity fold-change and single-cell distributions expressed from DIAL promoters with different spacer lengths with co-transfected ZFa (VP16-ZF37) on plasmids into HEK293T cells, with (dark green) or without (light green) Cre (n = 3). Output gmean fluorescence intensity is normalized to the condition without Cre within each spacer length. Histograms show decreasing pre-excision expression for increasing spacer length, which generates the larger fold-change upon addition

of Cre. f, Output reporter mGL gmean fluorescence intensity fold-change and single-cell distributions expressed from the 203-bp DIAL promoter transfected with different ZFas bearing different TADs (ZF-TADs, for example, ZFa) on plasmids into HEK293T cells, with (dark) or without (light) Cre (n = 3). Output mGL gmean fluorescence intensity is normalized to the condition with VP16-ZF43 without Cre. Fold-change between -Cre and +Cre conditions within each ZFa is annotated on distributions. Fold-change increases with stronger ZFa. g. The nested DIAL promoter system with loxP (blue) and VloxP (purple) sites uses combinatorial inputs of ZFa, VCre and Cre to generate three promoter states and four different setpoints of expression. h, Logic table of inputs, ZFa, Cre and VCre, and outputs, promoter state, target setpoint and observed gene (mGL) expression for the nested DIAL promoter (n = 3). Single-cell distributions of output reporter from nested DIAL promoter with different input combinations transfected on plasmids into HEK293T cells. Different input combinations with the nested spacer enable four setpoints. i, Output reporter mGL gmean fluorescence intensity fold-change expressed from the nested DIAL promoter transfected on plasmids into HEK293T cells, with or without ZFa, Cre or VCre (n=3). Output mGL gmean fluorescence intensity is normalized to the condition with VP16-ZF43 without either recombinase. Fold change is also annotated between conditions. All units for fluorescence intensity are arbitrary units (a.u.). Fold-change is unitless. Large markers represent the mean of biological replicates (n = 3) with span indicating s.e.m. Single-cell distributions are sampled across bioreplicates.

To characterize the DIAL framework, we transfected a DIAL promoter containing a spacer length of 203 base pairs (bp) into HEK293T cells. We measured fluorescence using flow cytometry. To isolate transfected cells for analysis, we gated live, single cells based on expression of a co-transfection marker (Supplementary Figs. 1c and 2). Through a combination of ZFa and Cre inputs, we changed the molecular state of the 203-bp DIAL promoter to generate three unimodal output setpoints (Fig. 1c,d and Supplementary Figs. 1d and 3a). By co-expressing each ZFa with a fluorescent protein, we verified that the levels of ZFa do not change in the presence of Cre, indicating that differences in the DIAL output are not due to perturbations in levels of ZFa (Supplementary Fig. 3b,c). Using an antibody for the Flag-tag on the ZFa, we directly quantified the protein levels via western blot and

immunofluorescent staining with flow cytometry. Activation of Cre did not change ZFa levels (Supplementary Fig. 3d-f).

Cre-mediated excision of the spacer increases expression by reducing the distance between the binding sites and minimal promoter. We validated spacer excision via genotyping PCR. As expected, in the presence of Cre, a shorter band appears, corresponding to the edited promoter (Supplementary Fig. 4a,b). Further, addition of Cre in the presence of ZFa increases expression, reaching the level of a control promoter that lacks a spacer (Supplementary Figs. 1d and 5c,d). Using PCR analysis, we found there was a mixed population of pre- and post-edited promoters (Supplementary Fig. 4a,b). Even when DIAL was integrated at low copy and cells were sorted for Cre delivery, we observed mixed promoter states, indicating the activity of Cre limits



editing (Supplementary Fig. 4e–g). Nonetheless, the DIAL reporter exhibits uniform shifts in single-cell distributions, indicating efficiency does not substantially limit performance.

Next, we explored tuning the setpoints and range of the DIAL promoter. In synthetic promoter systems, expression increases as the distance between the transcription factor binding sites and the transcription start site decreases ³⁵. We hypothesized that increasing the length of the excisable spacer will reduce expression of pre-excision setpoint, resulting in a larger fold-change between the low and high DIAL setpoints. For a panel of spacers ranging in length from 27 bp to 263 bp, increasing spacer length decreases pre-excision output expression and increases the fold-change (Fig. 1e and Supplementary Figs. 4c,d and 5a–d). Expression from the post-excision setpoint converges to the control construct which represents the post-excision sequence (Fig. 1e and Supplementary Fig. 5c,d).

Through tessellation of binding sites, the DIAL promoter responds to ZFas with either ZF37 or ZF43 binding domains (Supplementary Fig. 1a), allowing us to modularly combine domains of ZFs and TADs to generate ZFas of different strengths³⁵. We found that increasing the strength of the ZFa modestly increases the setpoint and fold-changes (Fig. 1f and Supplementary Fig. 5e,f). The strongest ZFa, VPR-ZF37, substantially increases setpoint levels and the range. However, in some cases, VPR-ZF37 generates bimodal expression of the reporter, which may be linked to toxicity and limit its utility for experiments requiring uniform control (Fig. 1f and Supplementary Fig. 3f). For the ZFas that generate unimodal setpoints, recombinase-mediated editing of the promoter generates a larger fold-change compared with exchange of the ZFas.

To investigate the flexibility of minimal promoter choice in DIAL, we tested a set of minimal promoters placed downstream of the ZFa binding sites using the 203-bp spacer⁴². Across the set, expression increases upon addition of Cre (Supplementary Fig. 6a). The choice of minimal promoter influences the levels of pre- and post-excision expression, fold-change and basal activity, as well as the shape of the single-cell distributions (Supplementary Fig. 6a,b). As the exact cell type may vary by application, minimal promoters may behave differently across cell types and provide flexibility to tune the DIAL output.

To increase the number of setpoints from a single promoter, we nested a set of orthogonal recombinase sites to generate multiple excisable spacers (Fig. 1g and Supplementary Fig. 7a-c). VCre, an orthogonal tyrosine recombinase, recognizes and excises regions flanked by VloxP sites. Addition of internal VloxP sites within the original floxed spacer allows promoter editing to generate three promoter states (Fig. 1h). Addition of VCre excises the shorter, VloxP-flanked spacer, increasing the setpoint from low to medium expression. Addition of Cre excises the entire floxed spacer, inducing the high setpoint. In the absence of ZFa, DIAL expression is OFF. Through combinations of specific recombinases and ZFa, we generate four defined setpoints that span more than an order of magnitude from a single promoter construct (Fig. 1i and Supplementary Fig. 7d-h).

DIAL setpoints are robust to varying levels of ZFa

Cellular physiology and the process of gene regulation contribute to variability in the expression of transgenes $^{43-45}$. High variability in the expression of components can lead to poor performance of gene circuits 31,32,46 . Ideally, circuits can be designed to buffer variation and ensure robust performance across populations and over time $^{5,47-51}$. For synthetic transcription factor systems, low expression of transcription factors contributes to bimodality, which is often masked by observation of only the mean level of the population 32 (Fig. 2a). As bimodality contributes to poor control and circuit performance, promoter systems ideally generate unimodal expression of transgenes.

Potentially, sufficient expression of transactivators can establish regimes that are unimodal and invariant to transactivator levels^{32,33}.

To examine the sensitivity of DIAL to variation in the levels of ZFa, we performed a titration of two ZFas (Fig. 2b-d and Supplementary Fig. 8a-c). Using fluorescent markers, we measured the transgene output from the 203-bp DIAL promoter for varying levels of ZFa.

At high levels of ZFa, the mean expression from the DIAL promoter remained constant at the induced setpoint (Fig. 2d and Supplementary Fig. 8b). In this dosage-invariant regime, the DIAL setpoints are maintained even while the level of ZFa ranges over one order of magnitude (Fig. 2d and Supplementary Fig. 8b). This dose-invariant regime likely reflects promoter saturation. At lower ZF levels, bimodality emerges. As ZF levels decrease, the overall population mean decreases due to the increasing population of cells in the OFF state (Fig. 2b,d and Supplementary Fig. 8b,c). The bimodality may result from factors such as delivery efficiency of the ZFa (Supplementary Fig. 9). Isolating the cells expressing the output gene, we find that DIAL expression is invariant to levels of ZFa for both the high and the low setpoints (Fig. 2e and Supplementary Fig. 8d). At lower ZFa levels, the fraction of reporter-positive cells changes, but the mean of the positive cells remains unchanged (Supplementary Fig. 8e). While changing the levels of ZFa does not uniformly change expression, DIAL provides a mechanism to uniformly increase the setpoint of expression via promoter editing.

To quantitatively characterize DIAL, we used a model of transcriptional activation. This model uses a simple Hill function to capture ZFa binding and the rate of transcriptional activation of the ZFa-bound promoter. Using the plasmid titration data, we fit the input ZFa and output expression for each condition in the presence or absence of Cre (Fig. 2d,g and Supplementary Fig. 8i). Although this model does not capture bimodality, comparison of the fitted parameters for the mean reporter outputs allows us to quantify the effect of promoter editing on the estimated binding affinity and rate of transcriptional activation. As expected, the binding affinity of the ZFa does not show a substantial change upon excision of the spacer via Cre (Supplementary Tables 3 and 4 and Supplementary Fig. 8j). However, decreasing the distance between the ZFa binding sites and minimal promoter increases the putative rate of transcriptional activation up to 15-fold (Supplementary Tables 3 and 4 and Supplementary Fig. 8j). In RNA-fluorescence in situ hybridization (RNA-FISH) measurement of output messenger RNA, we find that DNA editing increases transcript levels only fivefold, suggesting editing may influence other steps in expression such as RNA processing and export (Supplementary Fig. 10)52.

As DIAL is robust to ZFa levels, DIAL setpoints should be flexible to the choice of promoter, opening the potential to layer control around ZFa induction. Provided ZFa levels reach the dosage-invariant regime, DIAL should generate the predicted setpoints. Using constitutive promoters of different strengths, we generated a range of ZFa expression levels (Fig. 2f and Supplementary Fig. 8f). Changing the expression of ZFa via the selection of the ZFa promoter provided us an independent method to examine the predictions of DIAL setpoints based on ZFa expression. Consistent with the plasmid titration, output from the DIAL promoter is uniform across the range of ZFa, matching the predictions made by our model (Fig. 2g,h and Supplementary Fig. 8g,h). Within the dosage-invariant regime, DIAL generates predictable, programmable and highly robust unimodal setpoints, opening opportunities to layer control around system components.

DIAL transmits transient inputs into heritable states

Transmitting transient events into heritable states supports event recording and stable direction of cell trajectories ^{53–56}. As editing of the DIAL promoter is recorded in the DNA, these changes in promoter state can be transiently induced and then inherited, allowing cells to generate long-term trajectories from a temporally defined stimulus. We explored three methods of transiently inducing DIAL setpoints and tracked the heritability of DIAL when integrated (Fig. 3a).

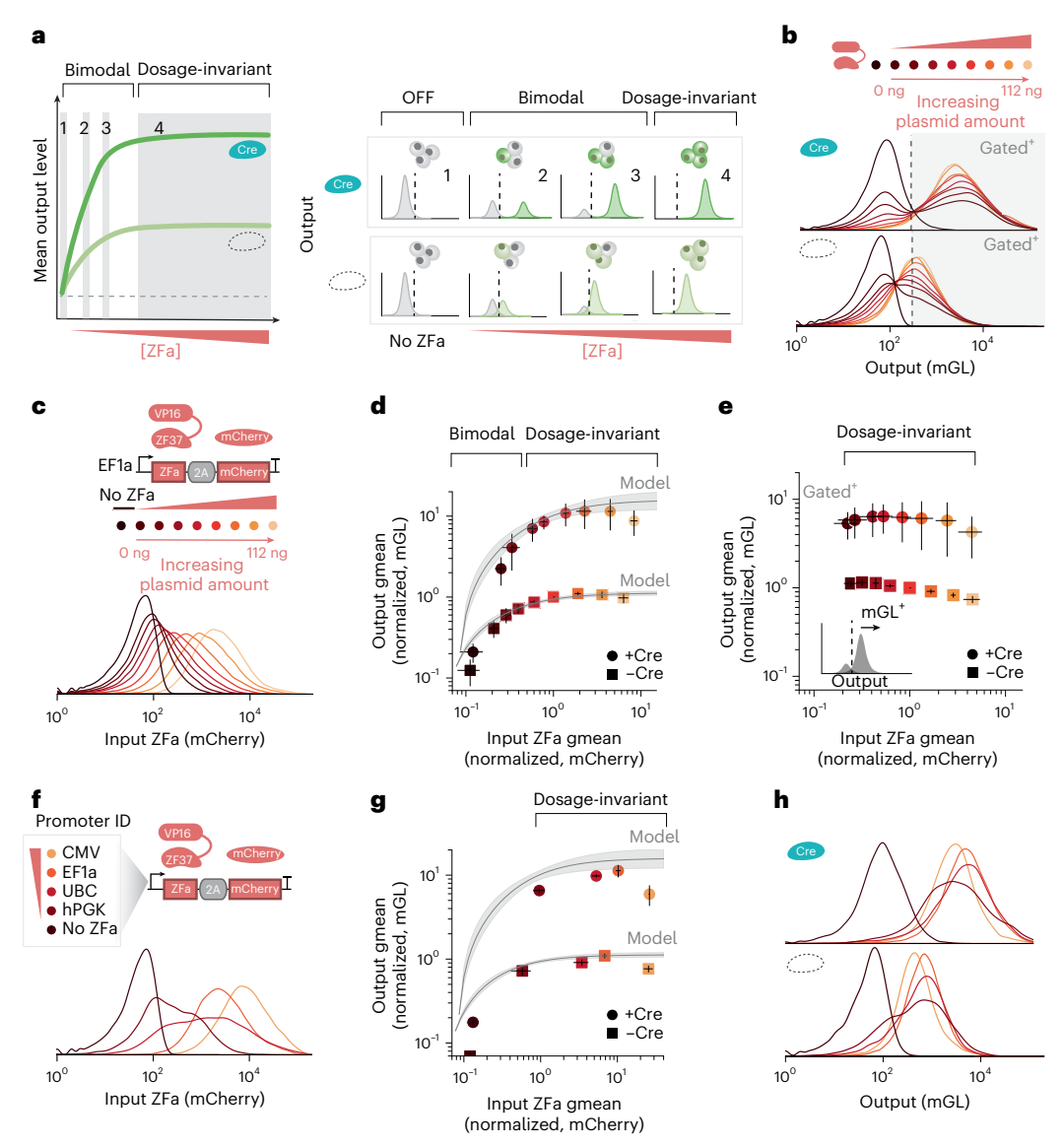


Fig. 2 | DIAL setpoints are robust to varying levels of transcription factor.

a, Mean expression from synthetic promoters increases in response to varying levels of transcription factors. At low levels of ZFa, synthetic promoters such as DIAL generate a bimodal output, but above a threshold of ZFa level, the output levels enter a dosage-invariant regime where output does not vary as ZFa varies. In the dosage-invariant regime, promoter editing changes the unimodal setpoint. b, Output mGL single-cell distributions expressed from the 203-bp DIAL promoter titrated with ZFa (VP16-ZF37) transfected on plasmids into HEK293T cells with or without Cre (n = 4). The gate is drawn to isolate populations with high output levels of the DIAL promoter. In the presence of Cre, the output mGL increases. At low levels of ZFa, output mGL is bimodal. c, Input mCherry singlecell distributions co-expressed with titrated ZFa (VP16-ZF37) in b transfected on plasmids into HEK293T cells with 203-bp DIAL promoter regulating mGL (n = 4). Conditions with and without Cre are combined. Schematic shows the plasmid titration of ZFa. d, Output reporter mGL gmean fluorescence intensity expressed from 203-bp DIAL promoter versus input ZFa gmean fluorescence intensity (proxied by co-expressed mCherry) for ZFa titration shown in b and c with and without Cre (n = 4). Values are normalized to the condition without Cre with 0.125× ZFa (14 ng of ZFa). Overlaid lines represent model fit with 95% confidence interval. The output initially increases at low ZFa levels, where the distribution is bimodal, followed by a dosage-invariant regime. e, Output reporter mGL

gmean fluorescence intensity (gated* by the line in **b**) versus input ZFa gmean fluorescence intensity (proxied by co-expressed mCherry, as shown in c not gated⁺ for mGL) for ZFa titration shown in **b** and **c** with and without Cre (n = 4). Values are normalized to the condition without Cre with 0.125× ZFa (14 ng of ZFa). Once gated, the reporter output is dosage-invariant throughout the ZFa plasmid titration. f, Input mCherry (proxy for ZFa VP16-ZF37) single-cell distributions expressed from constitutive promoters of varying strengths transfected on plasmids into HEK293T cells with 203-bp DIAL promoter regulating mGL (n = 3). Conditions with and without Cre are combined. g, Output reporter mGL gmean fluorescence intensity expressed from 203-bp DIAL promoter versus input ZFa (VP16-ZF37) gmean fluorescence intensity (proxied by co-expressed mCherry) expressed from different strength promoters transfected on plasmids into HEK293T cells with or without Cre (n = 3). Output values are normalized to the condition without Cre with EF1a promoter. Input values are normalized to without Cre with 0.125× ZFa (14 ng of ZFa) in d. Colored according to legend in f. h, Output mGL single-cell distributions expressed from 203-bp DIAL promoter when using different promoters to control ZFa transfected on plasmids into HEK293T cells, with and without Cre (n = 3). Conditions correspond to \mathbf{f} and \mathbf{g} . All units for fluorescence intensity are a.u. Normalized values are unitless. Large markers represent the mean of biological replicates $(n \ge 3)$ with span indicating s.d. Histograms represent single-cell distributions sampled across bioreplicates.

We examined the stability of DIAL in response to a transient stimulus delivered by nucleoside-modified mRNA (modRNA) encoding the recombinase. While plasmid transfection works well for delivery of recombinases in model cell lines, modRNA offers a simple method for

transient in vitro and in vivo delivery of recombinases to diverse cell types ⁵⁷⁻⁵⁹. Delivery of modRNA encoding the Cre recombinase increases expression from DIAL in a fraction of the cells (Supplementary Fig. 12a). To characterize the dynamics of induction upon Cre activity, we

integrated the DIAL system into HEK293T cells using separate lentiviruses to deliver the activator and the 203-bp DIAL promoter regulating mGreenLantern (mGL) (Supplementary Fig. 11a). We co-delivered Cre and mRuby2-P2A-PuroR modRNA to this polyclonal HEK293T population and measured fluorescence using flow cytometry over 14 days. At 15 h, we could detect expression of modRNA-delivered mRuby2 which peaked at 24 h (Supplementary Fig. 11b,d). The shift in target gene expression from the DIAL promoter begins at 24 h, and stabilizes around 72 h (Supplementary Fig. 11c,e). The induction of DIAL to the new setpoint coincides with the peak expression from the modRNA. To examine stability, we continued this experiment to 14 days post transfection (dpt). By 5 dpt, expression of mRuby2 reaches background levels, indicating dilution of the modRNA-delivered protein (Supplementary Fig. 11d). However, as expected, expression of the target gene remains high at 5 dpt; the difference between conditions that do and do not receive modRNA persists to 14 dpt (Supplementary Fig. 11e).

To examine heritability of the DIAL setpoint changes from Cre expression, we serially passaged a DIAL-integrated cell line following modRNA Cre delivery (Fig. 3b). To estimate dilution of Cre over serial passaging, we co-delivered modRNAs encoding Cre and a fluorescent protein (TagBFP) (Fig. 3c). By 9 dpt, TagBFP levels dropped to background levels. Nonetheless, at 9 dpt, we still observe a clear separation between the populations with high and low setpoints, indicating the DIAL promoter state is heritable over this period (Fig. 3d and Supplementary Fig. 12b). However, the mean expression of the population that received modRNA Cre decreases with time, which likely reflects the expansion of unedited cells and not transgene silencing³¹. Higher expression of transgenes can induce cellular burden and reduce proliferation ^{26,28-30}. If unedited cells expand in the condition that received Cre, we would expect an increase in the fraction of cells at the lower peak, matching the expression level of the unedited cells. Conversely, transgene silencing would broadly reduce expression of the setpoints. The increase in the fraction of the population at the low setpoint suggests the loss of cells at the high setpoint reflects the combined effects of fractional editing and transgene burden (Fig. 3e). The level of the higher peak does not substantially change over the 9 dpt, supporting heritability of the setpoint from the edited promoter state. Separate from this effect, we observe an increase in the population of mGL-negative cells from 9% to 25%, which may reflect transgene silencing or competition (Supplementary Fig. 12c,d). Nonetheless, we retain distinct low and high setpoints. Loss of cells at the high setpoint over time suggests competition between these two populations (Supplementary Fig. 12d). In separate experiments, we observed a similar decrease in the fraction of cells at the high setpoint despite low rates of silencing, suggesting that competition favors the low setpoint (Supplementary Figs. 13 and 14). Overall, these data indicate that DIAL can induce heritable expression changes that can be tracked over multiple rounds of cell division. Importantly, DIAL generates a dose-dependent selection effect, indicating that DIAL may support identification of transgenes with subtle effects on proliferation.

For genetically engineered model organisms and in vivo applications where stable integration of reporter and recombinase expression may be desirable, small-molecule control of Cre and ZFa offers a simple method for adjusting the DIAL setpoint. Cre-mediated editing can be induced via small molecules and light⁶⁰. Addition of gibberellin (GIB) induces Creactivity via chemical-inducible dimerization domains tethered to halves of the split Cre recombinase⁶⁰. In transfection, addition of GIB in the presence of ZFa increases expression of the reporter (Supplementary Fig. 15). Small-molecule control of recombinases can also be combined or exchanged for small-molecule control of the ZFa. DIAL relies on expression of the ZFa. Thus, inducible, pathway-responsive and cell-type-specific promoters that induce ZFa expression provide an additional method to selectively activate DIAL. Small-molecule-induced expression of the ZFa provides a reversible mechanism to induce expression at the setpoint defined by the promoter state. To demonstrate inducible control of DIAL, we encoded the ZFa under the DOX-inducible TRE3G promoter. As expected, combinations of DOX and Cregenerate three setpoints of expression (Supplementary Fig. 16). Unlike promoter editing with Cre, small-molecule induction of ZFa does not provide inherited memory via editing. Removal of DOX returns expression to the OFF setpoint. Both activation and editing of DIAL can be controlled by small molecules to allow conditional induction of setpoints via the choice of DOX and GIB (Fig. 3f-i and Supplementary Fig. 17). Smallmolecule control retains independent induction of setpoints while supporting uniform delivery of the full DIAL system at a single timepoint. Altogether, DIAL setpoints can be changed and induced at userdefined timepoints through transient stimuli.

Integration of the TET-On system into the DIAL framework enables small-molecule activation at defined setpoints

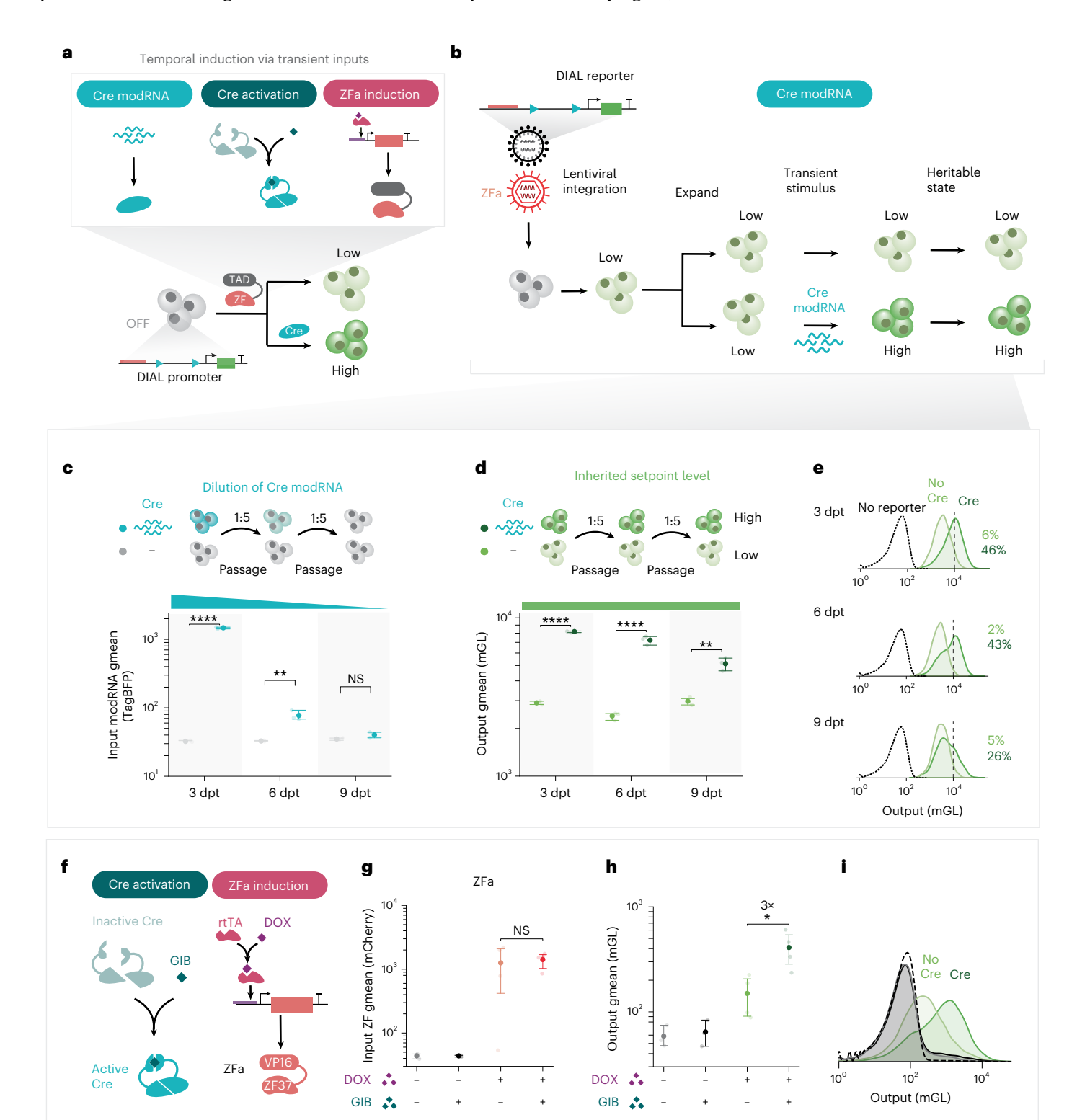
We hypothesized that the DIAL framework could be expanded to other transactivator systems that use upstream binding sites to

Fig. 3 | DIAL transmits transient inputs into heritable states. a, DIAL can be regulated by different transient and temporally defined methods to regulate the activity and expression of Cre and ZFa inputs for DIAL. b, Process to generate a polyclonal HEK293T line to demonstrate heritability of DIAL setpoints. Following delivery of lentiviruses of ZFa (VP16-ZF37-2A-mCherry) and 203-bp spacer DIAL promoter regulating mGL, sorting mGL⁺ and expansion, transfection of Cre modRNA sets heritable setpoints of expression level. c, Input TagBFP gmean fluorescence intensity (expressed via transfected modRNA, proxy for co-delivered Cre modRNA). d, Output mGL expressed from the 203-bp DIAL promoter gmean fluorescence intensity. e, Output mGL single-cell distributions over multiple passages from the polyclonal HEK293T cell line in \mathbf{b} (n = 3). Conditions are with and without modRNA (co-transfected TagBFP and Cre). Cells are gated for mGL⁺ and mCherry⁺. Protein expressed from the co-transfected modRNA dilutes or degrades to background levels after multiple passages (by 9 dpt). The difference in mGL setpoint level between conditions persists across multiple passages. In the single-cell distributions, the dotted curve is for uninfected HEK293T cells with no reporter or ZFa integrated. The vertical line represents a gate to isolate the lower peak and the higher peak. The percentages indicate the fraction of cells above the gate for the conditions with (dark green) and without (light green) Cre modRNA. d, Output reporter mGL gmean fluorescence intensity from 203-bp DIAL promoter over multiple passages measured on 3, 6 and 9 dpt in a polyclonal HEK293T cell line as described in b. Conditions are with and without modRNA (co-transfected TagBFP and Cre), Cells are gated for mGL+ and mCherry+. The difference in mGL setpoint level between

conditions persists across multiple passages. e, Output reporter mGL single-cell distributions over multiple passages measured on 3, 6 and 9 dpt in a polyclonal HEK293T cell line as described in **b**. Conditions are with (dark green) and without (light green) co-transfected TagBFP and Cre modRNA at 0 dpt. Cells are gated for mGL⁺ and mCherry⁺. The dotted curve is a representative single-cell distribution of uninfected HEK293T cells with no reporter or ZFa integrated. The vertical line represents a gate to isolate the lower peak and the higher peak. The percentages indicate the fraction of cells above the gate for the conditions with (dark green) and without (light green) Cre modRNA. f, Schematic of GIB-inducible split Cre and DOX-inducible ZFa encoded by a TRE promoter. g, Input mCherry gmean fluorescence intensity expressed from TRE-VP16-ZF37-2A-mCherry. h, Output mGL gmean fluorescence intensity expressed from the 203-bp DIAL promoter. i, Output mGL single-cell distributions with or without DOX (1 µg ml⁻¹) and GIB (1 µM) (n = 3). The 203-bp DIAL promoter regulating mGL was transfected with GIBinducible split Cre, rtTA and TRE-VP16-ZF37-mCherry on plasmids into HEK293T cells. Distribution conditions are according to the legend in h. The distribution with the dotted line represents the single-cell distribution of untransfected cells. DOX turns input ZFa expression from 'OFF' to 'ON'. DOX turns output mGL expression 'OFF' or 'ON', whereas presence of GIB determines levels of 'ON' expression. All units for fluorescence intensity are a.u. Fold-change is unitless. Large markers represent the mean of biological replicates with span indicating s.e.m. Histograms represent single-cell distributions sampled across bioreplicates. Statistical significance was calculated with two-sided Student's *t*-test, with NS P > 0.05; *P < 0.05; *P < 0.05; ****P* < 0.001; ****P* < 0.0001. NS, not significant.

recruit transcriptional machinery to a core promoter. To test this hypothesis, we integrated the commonly used TET-On system into the DIAL framework. In the presence of DOX, the transactivator rtTA binds to the tet-responsive promoter composed of an array of tetO sites upstream of a minimal promoter, resulting in the expression of the downstream gene. Thus, the TET-DIAL system enables reversible, small-molecule-based induction of transgenes.

We hypothesized that incorporating the TET-On system into the DIAL framework would shift expression between unimodal setpoints while maintaining reversible, small-molecule-responsive induction. We constructed TET-DIAL by inserting a floxed spacer between the tetO sites and the minimal YB_TATA promoter (Fig. 4a,b). Across a range of spacer lengths, the addition of Cre increases output expression by up to fivefold over pre-excision levels (Fig. 4c-e and Supplementary Fig. 18a,b,d,e). The post-excision setpoint matches the level of expression of a control lacking a spacer, and we confirmed excision via PCR (Supplementary Fig. 18f). TET-DIAL can also be combined with GIB-inducible Cre for dual small-molecule control of induction and setpoint level (Supplementary Fig. 20).



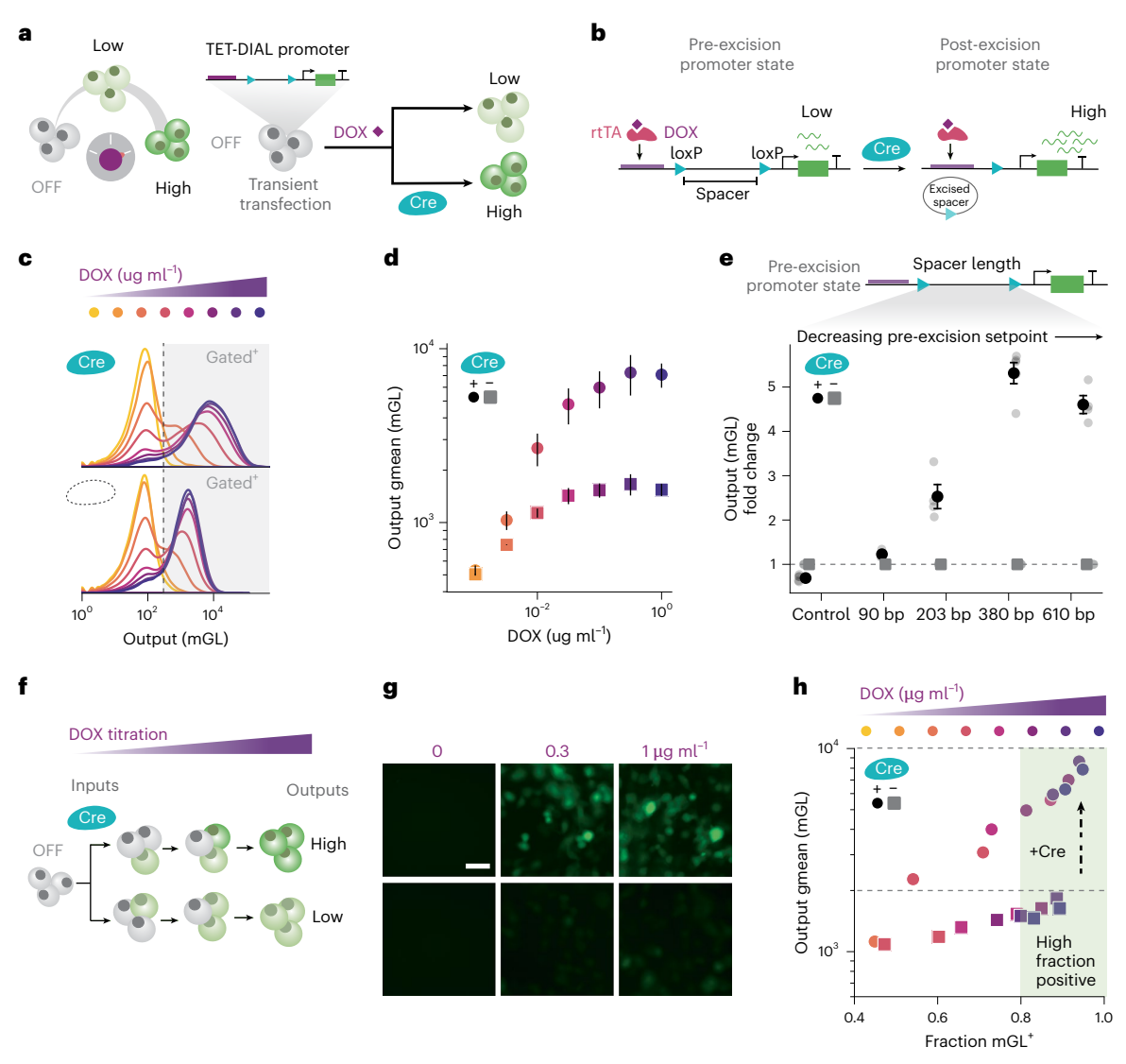


Fig. 4 | DIAL framework extends tunable setpoints across transactivator systems. a, In the presence of co-delivery with rtTA, the TET-DIAL promoter system uses combinatorial inputs of DOX and Cre to generate distinct setpoints of gene expression from a single promoter in transient transfection. b, Preexcision and post-excision states of the TET-DIAL promoter before and after Cre-mediated editing, respectively. The excision of the floxed spacer reduces the distance between the tetO sites and YB_TATA minimal promoter. c, Output reporter mGL single-cell distributions. d, Output gmean fluorescence intensity from the 610-bp TET-DIAL promoter regulating mGL with rtTA transfected on plasmids into HEK293T cells, with and without Cre (n = 3). DOX titration (1 µg ml⁻¹ titrated down) matches the colors in d, with the no DOX condition represented by the lightest yellow. Addition of Cre increases reporter expression, whereas titrating DOX results in concurrent changes in fraction of reporter-positive cells and expression level. Gate is drawn to isolate cells with expression above the no DOX condition (lightest yellow). e, Fold-changes of the output reporter mGL expressed from the TET-DIAL promoter of varying spacer lengths co-transfected with rtTA on plasmids into HEK293T cells with DOX $(1 \mu g ml^{-1})$ (n = 3 for 90-bp), n = 4 for 203-bp and 610-bp, n = 5 for 380-bp and control). Output mGL gmean fluorescence intensity normalized to the condition without Cre within each spacer length. Longer spacer lengths generate larger fold-changes upon addition of Cre. The 90-bp TET-DIAL promoter uses VloxP sites, and all others use loxP sites. f, DOX titration with the TET system leads to concurrent increase in fraction

of reporter-positive cells and mean expression level. Promoter editing in DIAL allows changing setpoints with high DOX concentration, hence maintaining a high fraction positive. g, Representative fluorescence microscopy images of output mGL expression from 610-bp TET-DIAL promoter co-transfected with rtTA on plasmids into HEK293T cells, with or without Cre, at 0, 0.3 and 1 µg ml⁻¹ DOX concentrations (n = 3). Images taken at 3 dpt. Scale bar, 20 μ m. **h**, Output reporter mGL gmean fluorescence intensity of the gated positive population versus the fraction of cells gated positive from the 610-bp TET-DIAL with rtTA cotransfected on plasmids into HEK293T cells, with or without Cre. Points represent individual bioreplicates (n = 3). Gate drawn (mGL > 200) to isolate populations with output fluorescence above condition without DOX. DOX concentrations match the corresponding colors in d. Dashed lines separate low and high reporter expression regimes. TET-DIAL allows for a shift between a low and high reporter expression state via promoter editing without a substantial effect on the fraction of mGL-positive cells. To set unimodal expression levels (OFF, Low, High) with high fraction positive in the 'ON' state, presence of DOX at high concentration can control whether expression is 'OFF' or 'ON', and presence of Cre can control the level of the 'ON' expression. All units for fluorescence intensity are a.u. Foldchange is unitless. Large markers in **d** and **e** represent the mean of biological replicates $(n \ge 3)$ with span indicating s.d. (d) or s.e.m. (e). Histograms represent single-cell distributions sampled across bioreplicates.

Similar to DIAL, we observed that the output profile of TET-DIAL generates two distinct regimes of modality. At low levels of DOX, TET-DIAL generates a bimodal output whereas at higher levels of DOX the output is unimodal and insensitive to changes in DOX (Fig. 4c,d and

Supplementary Fig. 18a,b). Addition of Cre increases expression across DOX concentrations. As with ZFas, titrating the levels of the rtTA generated bimodal expression (Supplementary Fig. 19). Increasing DOX concentration concurrently changes the mean expression and the fraction

of the reporter-expressing cells (Fig. 4f–h and Supplementary Fig. 18c). Alternatively, Cre editing of the TET-DIAL promoter allows us to independently change the setpoint without substantially changing the fraction of induced cells.

For TET-DIAL, we also investigated different minimal promoters with the 203-bp spacer. We sampled a panel of four additional minimal promoters (Supplementary Fig. 21). All minimal promoters tested showed an increase in expression upon addition of Cre. As with DIAL, the choice of minimal promoter also influences the levels of pre- and post-excision expression as well as the shape of the single-cell distributions.

Overall, TET-DIAL enables unimodal shifts in output setpoint via promoter editing while retaining the reversibility and temporal control offered by small-molecule induction. Expanding the DIAL system to additional transactivator systems suggests that the DIAL framework serves as an extensible framework for building robust setpoints from a single promoter construct.

DIAL is portable to primary cells and iPSCs and regulates diverse transgenes

For the broadest impact across research and therapeutics, genetic control systems need to perform in primary cells and human iPSCs. To characterize DIAL performance in primary cells, we delivered DIAL promoters via lentivirus into mouse embryonic fibroblasts (MEFs) (Fig. 5a). Combinations of ZFa and Cre were delivered via retroviruses. As expected, the addition of Cre increases the DIAL setpoint without affecting ZFa expression (Fig. 5b,c and Supplementary Fig. 22a-f). The longer spacer and the stronger ZFa generate a larger range between setpoints (Fig. 5b and Supplementary Fig. 22a,c). For temporal control of output expression in MEFs, we encoded the ZFa under the control of a DOX-inducible TRE3G promoter on a lentivirus that constitutively expresses the rtTA transactivator (Fig. 5d). We delivered the DIAL promoter on a separate lentivirus. As expected, delivery of Cre via retrovirus increases expression without affecting ZFa levels (Fig. 5d and Supplementary Fig. 22g,h). Addition of DOX induces expression of the ZFa, activating expression from DIAL at low and high setpoints based on the presence of Cre (Fig. 5d).

Next, we tested a range of DIAL promoters in human iPSCs (Fig. 5e). We transfected the 203-bp DIAL promoter, the nested DIAL promoter and the 380-bp TET-DIAL promoter into iPSCs with combinations of

ZFas and recombinases. As expected, addition of ZFa induces expression, and recombinase-mediated editing increases the setpoint (Fig. 5f and Supplementary Fig. 23a,d). The nested DIAL promoter generates four setpoints of expression (Fig. 5g and Supplementary Fig. 23b,e). For the 380-bp TET-DIAL promoter, addition of DOX induces expression and recombinase-mediated editing increases the setpoint (Fig. 5h and Supplementary Fig. 23c). Thus, DIAL provides a toolkit that performs across a range of cell types.

Genetic controllers should be able to regulate arbitrary genes to execute titrations, enable screening and enact diverse control functions. To demonstrate that DIAL can control expression of functionally relevant genes, we encoded the tumor suppressor protein p53, encoded by the *Trp53* gene, and HRas^{G12V}, an oncogenic mutant of the *HRAS* gene, under the control of the DIAL promoter. To visualize expression and measure setpoints, we fused *Trp53* to Halo, a ligand-controlled self-labeling protein tag, and *HRAS*^{G12V} to the fluorescent protein mCherry. As expected, DIAL generates unimodal setpoints of expression of the fusion proteins Halo–p53 and mCherry–HRas^{G12V} without affecting ZFa level (Fig. 5i, j and Supplementary Fig. 24). Further, DIAL regulates multiple genes by controlling expression of polycistronic cassettes (Fig. 5k and Supplementary Fig. 24). In summary, DIAL generates setpoints of expression for arbitrary genes and in diverse cell types, supporting both research and translational applications.

DIAL generates stable setpoints to drive distinct phenotypes and fates

Transgenes can drive cells to transition identities ¹⁻⁶. For dosage-sensitive regulators of fate, the frequency of transition increases (or decreases) as levels of these regulators increase ⁶¹⁻⁶³ (Fig. 6a). For instance, increasing the levels of the MAPK mutant HRas ^{G12V} increases rates of the conversion of fibroblasts to induced motor neurons (iMNs) ⁶¹. Identifying dose-sensitive regulators remains a challenge as variations in cellular physiology, as well as transgene design and delivery, can influence cells' states and fates ⁶¹. To map the dose–response curve of conversion to HRas ^{G12V} levels, we previously employed a large number of lentiviral constructs with different types of promoters and multiplicities of infection to generate distinct levels of HRas ^{G12V} and measure conversion ⁶¹. However, changing promoters to alter transgene expression can induce large variance in viral titer across constructs and produce different dynamics and distributions of expression in transduced cells ⁵².

Fig. 5 | DIAL regulates diverse transgenes and is portable to primary cells and iPSCs. a, Delivery of the DIAL promoter system via lentivirus to primary MEFs. a-c, The lentivirus encodes the DIAL promoter regulating mGL and a divergent EF1a-iRFP670. Retroviruses constitutively express Cre and ZFa and can be delivered in various combinations to set expression from the DIAL promoter. **b**, Single-cell distributions of output mGL (top) and fold-change (bottom) expressed from 155-bp or 203-bp DIAL promoters with divergent iRFP670 integrated into MEFs, with ZFa VP16-ZF37-2A-mCherry and with or without Cre (n = 5 bioreplicates from separate MEF batches at 3 dpi). The curves represent -ZFa, -Cre (gray); +ZFa, -Cre (light green); and +ZFa, +Cre (dark green). Foldchange is the output reporter mGL gmean fluorescence intensity normalized to the condition without Cre within each spacer length. In the presence of ZFa, fold-change is larger for longer spacer length. Cells are gated by iRFP670⁺. In the presence of ZFa, cells are additionally gated for mCherry*. c, Representative fluorescence microscopy images of mGL expressed from 203-bp DIAL promoter with divergent iRFP670 integrated into MEFs with ZFa VP16-ZF37-2A-mCherry, with or without Cre. Images taken 3 dpi. d, Output reporter mGL single-cell distributions (top) and gmean fluorescence intensity (bottom) expressed from 203-bp DIAL promoter with divergent iRFP670 on lentivirus infected into MEFs (n = 3 bioreplicates from separate MEF batches at 4 dpi). MEFs were co-infected with lentivirus of TET-VP16-ZF43-2A-TagBFP with divergent rtTA. Conditions are with or without DOX (1 μg ml⁻¹) and Cre retrovirus. The distributions are colored according to the plot legend. The presence of DOX turns on expression, and the addition of Cre unimodally increases expression from low to high. Cells are gated for iRFP670⁺. In the presence of DOX, cells are additionally gated for TagBFP⁺.

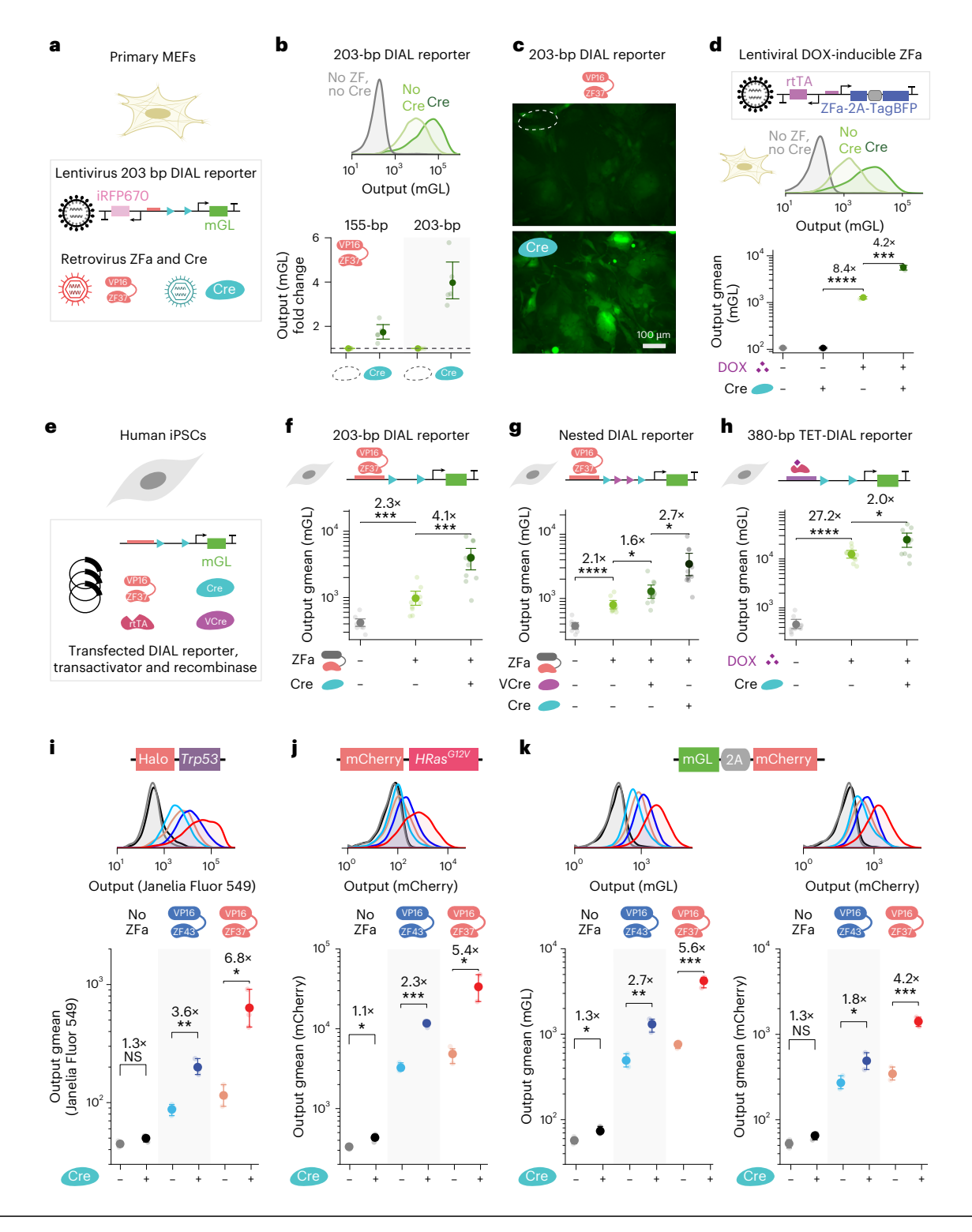
e, Schematic of various combinations of ZFa VP16-ZF37, VCre, Cre, rtTA and DIAL promoter transfected on plasmids into human iPSCs. f, Output reporter mGL $gmean\,fluorescence\,intensity\,expressed\,from\,203-bp\,DIAL\,promoter\,transfected$ on plasmids into iPSCs, with or without Cre and VP16-ZF37 (n = 11). Fold-change is between means. Output expression turns on in the presence of ZFa and increases upon addition of Cre.g, Output reporter mGL gmean fluorescence intensity from nested DIAL promoter transfected on plasmids into iPSCs, with or without VP16-ZF37, VCre and Cre (n = 10). Output expression turns on in the presence of ZFa and sequentially increases upon addition of VCre and Cre. h, Output reporter mGL gmean fluorescence intensity from 380-bp TET-DIAL promoter transfected with rtTA on plasmids into iPSCs, with or without DOX (1 μ g ml⁻¹) and Cre (n = 11). No output was observed in the absence of DOX, and +DOX conditions are gated for output-expressing cells. Output expression turns on in the presence of DOX and increases upon addition of Cre. i-k, Output reporter gmean fluorescence intensity from 203-bp DIAL promoter regulating different target genes (i, Halo-*Trp53*; **j**, mCherry–*HRas*^{G12V}; **k**, mGL-2A-mCherry) co-transfected on plasmids into HEK293T cells, with or without Cre and ZFa (VP16-ZF43 or VP16-ZF37). Across different target genes, output expression turns on in the presence of ZFa and increases upon addition of Cre. All units for fluorescence intensity are a.u. Foldchange is unitless and represents mean fold-change across bioreplicates. Large markers represent mean of bioreplicates with span indicating s.e.m. Histograms represent single-cell distributions sampled across bioreplicates. Statistical significance was calculated on bioreplicates with two-sided Student's t-test with, $NSP > 0.05; *P \le 0.05; **P \le 0.01; ***P \le 0.001.$

Different multiplicities of infection can also impact the percentage of infected cells and the copy numbers within infected cells, potentially obscuring the effects of varying expression levels on conversion rates. Through promoter editing, DIAL offers a simple, well-controlled framework for demonstrating a dose response from a single promoter delivered via the same batch of lentivirus (Fig. 6a). With DIAL, we can deliver identical amounts of virus, program stable, heritable setpoints via transient stimuli and examine how fine-scale changes in gene expression influence phenotypes and fates that emerge over weeks.

While DIAL generates stable outputs in cell lines and primary cells, generating setpoints that remain stable across a cell-fate transition presents a significant challenge for transgenic systems³¹. Rates

of transgene silencing increase over time and as cells differentiate, reprogram or convert identities 31,45,46,63-65. To examine the stability of DIAL setpoints across a cell-fate transition, we delivered DIAL-regulated mCherry–HRas GI2V lentiviruses to MEFs along with the conversion cocktail for iMNs (Fig. 6b). We used activation of the motor-neuron-specific Hb9::GFP transgenic reporter as a readout of conversion 45,61,66,67.

To generate the three distinct levels (OFF, Low and High) of mCherry–HRas G12V from a single DIAL promoter, we delivered conditions with and without ZFa or Cre. We tested delivery of Cre recombinase via modRNA (modCre) and retroviral GIB-inducible Cre (GIB-Cre) to allow small-molecule activation of Cre. We measured mCherry–HRas G12V fluorescence at 5 and 14 days post infection (dpi). Through



either small-molecule activation or modRNA delivery of the Cre recombinase, DIAL generates three distinct setpoints of mCherry–HRas^{G12V} by 5 dpi and maintains these setpoint differences to 14 dpi (Fig. 6c,d and Supplementary Figs. 25a and 26a). Notably, we also observed all three setpoints, OFF, Low and High, in cells gated for conversion to neurons (Hb9::GFP+ cells). Thus, the setpoints are stable across this cell-fate transition and allow investigation of functional differences over days and weeks.

As mCherry–HRas^{G12V} is a positive regulator of proliferation and conversion, higher expression setpoints should increase proliferation and generate greater iMN yield at 14 dpi (ref. 61). To measure proliferation history, we labeled cells at 1 dpi with a stable dye, CellTrace, and measured CellTrace fluorescence at 5 dpi along with mCherry expression (Supplementary Fig. 27a). Different batches of primary MEFs show differences in baseline proliferation. By normalizing within each batch of MEFs, we find that induction of higher mCherry–HRas^{G12V} levels via modCre or GIB-Cre delivery increases the number of cells with a history of hyperproliferation (Supplementary Figs. 25a, 26a and 27b,c). Importantly, these differences were not observed in the DIAL post-excision control promoter (Supplementary Figs. 25b, 26b and 27b,c).

To quantify yield, we counted Hb9::GFP-positive cells at 14 dpi and normalized to the number of cells seeded. As expected, increased expression of mCherry–HRas^{G12V} led to higher iMN yield (Fig. 6d and Supplementary Figs. 25a and 26a,c). Importantly, induction of the higher mCherry–HRas^{G12V} setpoint via recombinase delivery results in higher rates of conversion than at the lower setpoint for the same DIAL construct. As expected, Cre activity did not increase expression of mCherry–HRas^{G12V}, proliferation or conversion for the post-excision control (Supplementary Figs. 25b, 26b and 27).

TET-DIAL allows pulses of expression at different setpoints through addition and removal of DOX (Fig. 6e). We hypothesized that we could use TET-DIAL to simultaneously explore the effects of the mCherry-HRas^{GI2V} induction period and level. We used TET-DIAL to control expression of mCherry-HRas^{GI2V} and delivered modRNA Cre recombinase to generate different setpoints in the presence of DOX. By addition and removal of DOX, we achieved three different pulse lengths—short, medium and long—of mCherry-HRas^{GI2V} expression.

At 5 dpi, TET-DIAL generates distinct setpoints in response to DOX and Cre, unlike the TET-DIAL post-excision control promoter (Fig. 6f and Supplementary Fig. 28a). At 5 dpi, induction to the higher setpoint increases the number of hyperproliferative cells (Fig. 6g and Supplementary Figs. 28b and 29). At 14 dpi, the long pulse maintains setpoints in the bulk population and in iMNs (Hb9::GFP+ cells) (Fig. 6h and Supplementary Fig. 28). Withdrawal of DOX from the media at intermediate timepoints allows the levels of mCherry–HRas^{G12V} to return to the OFF state in a time-dependent manner (Fig. 6h).

With TET-DIAL, we could parse the effects of both HRas^{G12V} levels and duration on iMN yield. At 14 dpi, a medium pulse at the high setpoint generates higher yield than the low setpoint, but similar yield compared with the long pulse at either low or high setpoints (Fig. 6i). Thus, sustained induction of mCherry–HRas^{G12V} is not required to reach the highest yields of conversion. However, at the low setpoint, a long pulse increases yield compared with the medium pulse. Together, these data suggest that higher cumulative expression of HRas^{G12V} increases iMN yield. Future work may reveal how levels and duration of HRas^{G12V} expression influence the trajectories of single cells.

Overall, DIAL enables controlled delivery and titration of a cell-fate regulator to examine fine-scale effects on cellular phenotypes over long timescales. We use DIAL and TET-DIAL promoter editing to increase levels of mCherry–HRas^{G12V} and demonstrate setpoint stability during and after a cell-fate transition. Using TET-DIAL, we further identified an optimal expression duration, indicating that a transient pulse of mCherry–HRas^{G12V} can increase yield of iMNs.

Discussion

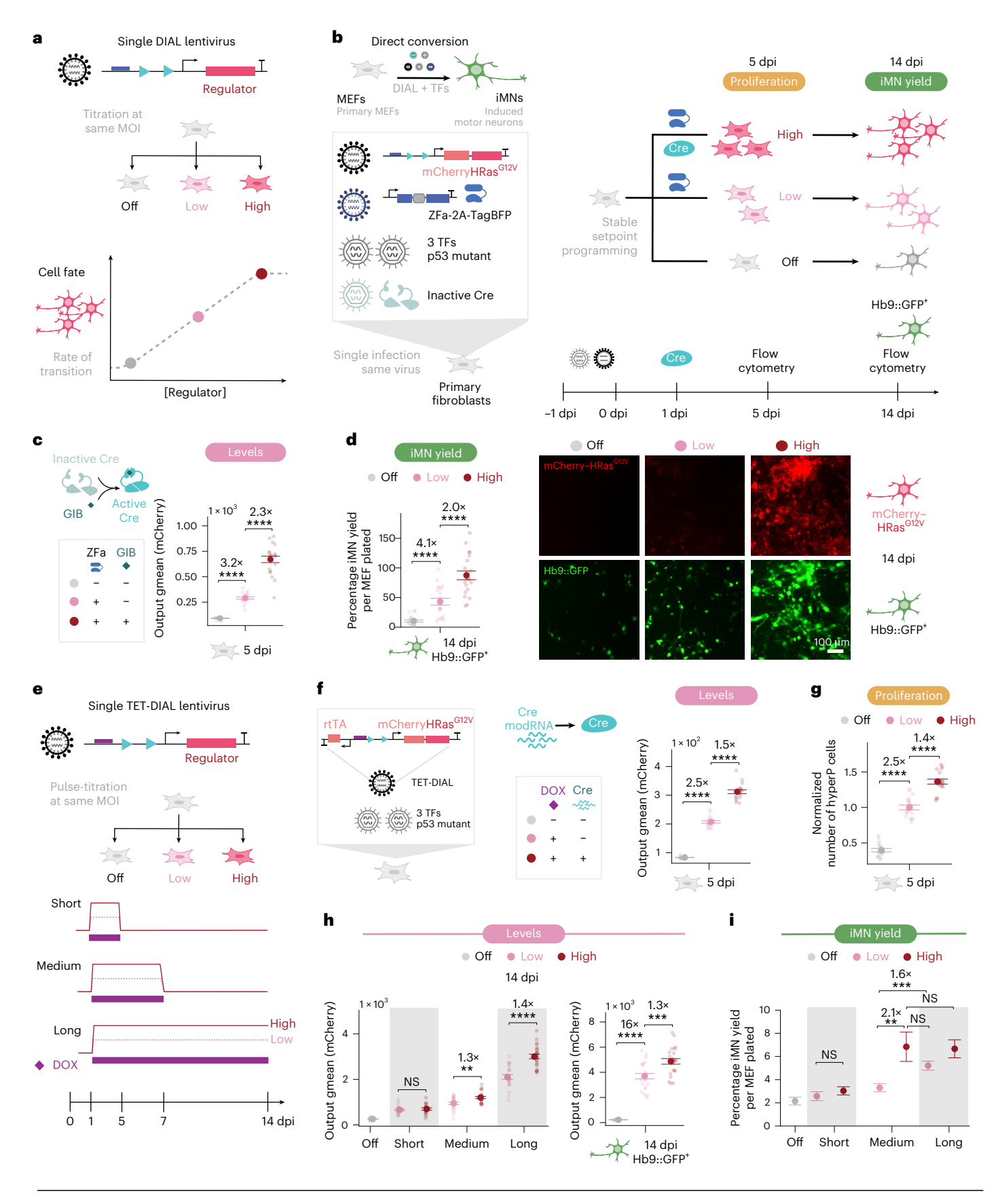
In this work, we present DIAL, a modular and extensible framework for engineering synthetic promoter systems. DIAL generates multiple unimodal setpoints of expression from a single promoter sequence (Figs. 1 and 2). Using the DIAL framework, we generate a toolkit of promoters responsive to diverse synthetic transcription factors with rationally tunable setpoints and ranges (Figs. 1 and 4). The multiple inputs of activator and recombinase allow combinatorial control of output level between OFF, Low and High setpoints (Figs. 1, 3 and 4). We demonstrate that recombinase-mediated editing of the DIAL promoter increases the

Fig. 6 | DIAL setpoints map fine-scale changes in regulator expression to rates of cell-fate transitions. a, For dosage-sensitive positive regulators of fate, the frequency of transition increases as levels of these regulators increase. A single DIAL promoter generates setpoints at distinct levels which can be mapped to rates of cell-fate transitions. b-d, DIAL generates distinct setpoints of mCherry-HRas^{G12V} during the conversion of MEFs to induced motor neurons (iMNs). MEFs are infected with the conversion cocktail consisting of three motor-neuronspecific transcription factors (3 TFs; Lhx3-Ngn2-Isl1) and a p53 mutant. The 380-bp DIAL promoter regulates the MAPK mutant HRas G12V fused to mCherry. DIAL activity is induced by the presence of the ZFa (VP16-ZF37-2A-TagBFP) and promoter editing is controlled via the GIB-inducible split Cre. Phenotypes and expression levels are measured at 5 dpi for proliferation and at 14 dpi for iMN yield. Conversion to iMNs is measured via activation of the motor neuron Hb9::GFP reporter from primary transgenic Hb9::GFP MEFs. b, Schematic of MEFto-iMN cell fate conversion. c, Output mCherry-HRas G12V gmean fluorescence intensity at 5 dpi. The OFF (gray), Low (pink) and High (red) setpoints are generated by combinations of ZFa and GIB (1 μ M). d, Percentage iMN yield per MEF plated and images of mCherry-HRas G12V and Hb9::GFP iMNs at 14 dpi. mCherry-HRas^{G12V} is regulated by the 380-bp DIAL promoter with the inputs and setpoints from c. Percentage yield is defined as the number of Hb9::GFP+ cells at 14 dpi divided by the number of cells seeded. Scale bar, 100 μm. e, A single TET-DIAL promoter generates pulses of expression at various setpoints, controlling for variation in delivery. Different durations of DOX treatment enable different length pulses at the low and high setpoints. DOX was added from 1 dpi to 5 dpi, 7 dpi or 14 dpi to generate short, medium or long pulses, respectively. f-i, MEFs are infected with the conversion cocktail consisting of three motor-neuronspecific transcription factors (3 TFs; Lhx3-Ngn2-Isl1) and a p53 mutant. The 380bp TET-DIAL promoter regulates the MAPK mutant HRas $^{\scriptsize G12V}$ fused to mCherry.

TET-DIAL activity is induced by the presence of DOX (1 μg ml⁻¹) and promoter editing is controlled via Cre modRNA. A control modRNA, eeBxb1, is added to conditions +DOX. -Cre. Phenotypes and expression levels are measured at 5 dpi for proliferation and at 14 dpi for iMN yield. Conversion to iMNs is measured via activation of the motor neuron Hb9::GFP reporter from the primary transgenic Hb9::GFP MEFs. Percentage yield is defined as the number of Hb9::GFP cells at $14\,dpi\,divided\,by\,the\,number\,of\,cells\,seeded.\,\textbf{\textit{f}},Output\,mCherry-HRas^{\tiny G12V}\,gmean$ fluorescence intensity at 5 dpi. The off (gray), low (pink) and high (red) setpoints are generated by combinations of DOX and Cre modRNA. g, Normalized number of hyperproliferative (hyperP) cells at 5 dpi for the conditions and legend in ${\bf f}$. Normalization is performed within each MEF batch. Each replicate is divided by the mean number of hyperP cells across all replicates for each batch. h, Output mCherry-HRas^{G12V} gmean fluorescence intensity 14 dpi for off (no DOX), short, medium and long pulses of DOX for all cells (left), and for off or long pulse of DOX conditions gated for Hb9::GFP+ cells (right). Withdrawal of DOX at intermediate timepoints allows the levels of mCherry–HRas G12V to return to the off state in a time-dependent manner. i, Percentage iMN yield for short, medium and long pulses of DOX and off, low and high mCherry-HRas GI2V levels. All units for fluorescence intensity are a.u. Fold-change is unitless and annotated as the difference between means of conditions. For DIAL and GIB-Cre, conversion experiments were conducted with four separate MEF batches with three to six replicates each (n = 21). For TET-DIAL and Cre modRNA, conversion experiments were conducted with three separate MEF batches with six replicates each (n = 18). Large markers represent the mean of replicates with span indicating s.e.m. Statistical significance was calculated with two-sided Student's t-test, with NS P > 0.05; *P < 0.05; **P < 0.01; ****P < 0.001; ****P < 0.0001. MOI, multiplicity of infection; TF, transcription factor.

setpoint of the target gene. DIAL can translate transient, user-defined inputs into heritable changes in the setpoint, supporting flexibility on the timing of setpoint changes (Fig. 3). For broad application, we show that DIAL can regulate physiologically relevant transgenes and

performs across diverse cell types including human iPSCs and primary murine cells (Fig. 5). Finally, using a positive regulator of cell-fate conversion, we show that DIAL can generate stable setpoints that drive cells to new fates at different rates (Fig. 6).



Precise programming of gene expression levels represents one of the most important and challenging goals in synthetic biology 68-71. While tools for control in mammalian systems have expanded over the last decade, few simple circuits have been translated clinically⁷⁰. In part, these limitations are driven by poor performance in primary cells and emergent behaviors such as bimodality and transgene silencing^{31,32,46}. We demonstrate that titration of synthetic transcription factors changes the fraction of cells in the 'ON' population but does not change the mean expression of the 'ON' population (Fig. 2). Alternatively, promoter editing via DIAL generates distinct unimodal setpoints of expression. DIAL setpoints are robust to variation of the synthetic transcription factor (Fig. 2). Over a tenfold range of transcription factor expression, DIAL output remains constant. In the TET-DIAL system, small-molecule titration of the DOX-inducible system slightly tunes the mean, but comes at the expense of changing the fraction of cells that express the output gene (Fig. 4). Via promoter editing, DIAL uncouples setpoints and bimodality, supporting independent tuning of the induced fraction of the population and the mean levels of expression. In the dosage-invariant regime, DIAL offers unimodal expression at programmable setpoints. The combination of unimodality and dosage-invariance to component variation indicates that DIAL will improve the predictability and performance of gene circuits.

The programmability, memory and stability of DIAL setpoints allowed us to examine how fine-scale changes in expression affect cell fates that emerge over weeks. Using DIAL, we controlled expression of HRas ^{G12V}, a positive regulator of proliferation and conversion of fibroblasts to iMNs^{61,67}, and showed that induction of the higher setpoint is stable through conversion and increases proliferation and conversion yields (Fig. 6). We used TET-DIAL to explore how transient induction of HRas G12V setpoints affects conversion rates. The transient induction of the high setpoint could generate yields of neurons similar to the continuous induction, aligning with our previous work indicating that early activity of HRas^{G12V} drives proliferation and conversion^{61,67}. Building on this work, we envision that DIAL could be used for similar fine-scale titration and for identification of dose-dependent regulators of cell phenotypes and fates over long time periods. The ability to use transient recombinase activity to program setpoint levels from a single promoter encapsulates one of the key advantages of DIAL. Unlike multiple constructs with constitutive promoters of different strengths, which introduce additional sources of extrinsic variation, DIAL minimizes extrinsic variation. By supporting the development of a single parental cell line and/or viral preparation. DIAL supports well-controlled systems to define the effect of transgene levels on phenotypes.

The DIAL framework allows integration of small-moleculeregulated synthetic transcription factors, indicating extensibility beyond ZF-based transcription factors. With TET-DIAL, we demonstrate the DIAL framework can be extended to the DOX-inducible system, supporting reversible, small-molecule-responsive induction (Fig. 4). As the field has developed an array of synthetic promoter systems 10,72, we envision that the DIAL framework could guide design of multiple unimodal setpoints in these systems. Similarly, integration of arrays of binding sites for diverse endogenous transcription factors into the DIAL framework may allow construction of tunable, cell-state-responsive promoters³⁶. Encoding the binding sites derived from pathway-responsive and tissue-specific promoters into DIAL may allow tuning of activity from these promoters and further support circuits for information processing, recording and computation of native signals^{25,73}. Our toolkit explores multiple core promoter sequences that change the pre- and post-excision setpoint levels, fold-change, basal activity without activator and shape of the single-cell distribution. Exchanging these sequences for other core promoters of different types may further tune the output and range from DIAL promoters 42,74. We observed that spacer length translated to output ranges that varied between the DIAL and TET-DIAL, suggesting that trends in spacer lengths may be preserved but the absolute length for optimal, desired range may vary by other

system features such as the synthetic transcription factor and core promoter. As contact between promoters and enhancers provides one mode of native gene regulation, it is interesting to speculate how DIAL might be used to study transcriptional dynamics⁷⁵. Potentially, decreasing the distance between the binding sites and core promoter increases the frequency of transcriptional bursts, as has been observed for forced enhancer looping and other synthetic transcription factor systems^{76,77}. As a well-defined system, DIAL provides a modular tool for parsing properties of gene regulation.

While recombinase systems have been used extensively for inducing expression, these systems primarily control binary states of expression (ON/OFF)^{54,60,78-80}. Other systems, such SCRaMbLE, GEMbLER and Genome-Shuffle-seg, have used recombinases to randomly recombine elements to generate diversity of expression for screening^{81–84}. In yeast, GEMbLER supports diversification of promoter sequences and expression profiles through random recombination of arrays of floxed endogenous promoters, leading to diverse expression levels⁸⁵. While such promoter recombination supports the identification of novel promoter combinations and optimal levels, random recombination does not support precise programming. While other systems have used recombinases to induce two different levels of expression through inversion of a bidirectional promoter⁸⁶, DIAL offers greater flexibility in tuning of fold-change, number of setpoint levels and cellular distribution through the variables of spacer length, nested recombinase sites, minimal promoter and transcription activator choice. With combinatorial control of transactivator and recombinase, DIAL generates an OFF setpoint in addition to Low and High setpoints. DIAL's ability to provide fine-scale tuning offers a unique application for tyrosine recombinases.

As more recombinases are discovered, characterized and engineered87,88, we expect that DIAL will expand to take advantage of additional recombinase properties and toolkits. Nesting recombinase sites within the spacer allowed us to access more expression levels from a single DIAL promoter (Fig. 1). Nesting additional orthogonal recombinase sites could expand the number of DIAL setpoints. Moreover, orthogonal sets of recombinases could also mediate independent control of setpoints for individual genes. Given the ubiquity of recombinase tools in model organisms and cell lines, DIAL may integrate with diverse recombinase-based tools for lineage tracing^{89–93}. We show that Creactivity can be instigated by orthogonal control systems, including external user-defined cues such as modRNA and small molecules, opening opportunities for changing setpoints at a specific timepoint^{60,94}. Similar to many Cre-based systems, Cre expression in the DIAL system could also be tied to diverse inputs via pathway-specific promoters for autonomous editing of setpoint levels.

While the DIAL framework provides many insights on engineering synthetic promoter systems, there remain limitations and opportunities to expand the capabilities. While DIAL setpoints are robust to synthetic transactivator level (Fig. 2 and Supplementary Fig. 8), other factors, such as the dosage of the DIAL promoter construct itself, may influence the setpoint. Alternative types of genetic controllers may provide control for variation in DNA dosage and other extrinsic factors 51,68,69,95-97. In its current form, DIAL allows us to increase setpoint levels, but not decrease the level of the setpoint, limiting application to systems where a reduction in the setpoint is needed. Although permanent DNA-level editing of DIAL offers stability and long-term, hereditable memory, setpoint changes are irreversible. TET-DIAL partially overcomes this limitation. Removal of DOX allows cells to return to the OFF state, but induction requires constant delivery of the small-molecule activator and edited promoter states remain irreversible. While many applications require fine-scale changes of transgene expression, the range of DIAL may be a limitation for some applications. Limited range may be a result of other DIAL features. In the current form of DIAL, we selected spacer sequences that we rationally identified as putatively neutral. A more expansive characterization may identify

sequence requirements for optimal performance of DIAL promoters. Finally, while we observed substantial shifts in expression and unimodal setpoints, the editing efficiency and delivery of recombinase presents a rate-limiting feature, motivating the development of high-efficiency enzymes and delivery methods ^{87,98,99}.

Overall, DIAL expands the mammalian cell engineering toolkit to achieve precisely programmable profiles of gene expression. With ZFa and TET binding sites, we offer a set of DIAL promoters with a variety of fold-changes and the ability to set multiple unimodal setpoints from a single construct. Control via a single promoter offers the scalability needed to generate multiple setpoints from libraries of transgenes and inherently controls for bias of clonal founder lines for a single transgene. Thus, DIAL may help identify and control transgenes with subtle dose-dependent effects on cellular states. Finally, we anticipate that the extensible framework offered by DIAL will support expansion to additional synthetic promoter systems and broadly improve precision cell engineering.

Online content

Any methods, additional references, Nature Portfolio reporting summaries, source data, extended data, supplementary information, acknowledgements, peer review information; details of author contributions and competing interests; and statements of data and code availability are available at https://doi.org/10.1038/s41587-025-02854-y.

References

- Domingo, J. et al. Nonlinear transcriptional responses to gradual modulation of transcription factor dosage. Preprint at bioRxiv https://doi.org/10.1101/2024.03.01.582837, peer reviewed by eLife eeb.embo.org/doi/10.1101/2024.03.01.582837 (2025).
- Wang, N. B. et al. Proliferation history and transcription factor levels drive direct conversion to motor neurons. Cell Syst. 16, 101205 (2025).
- Kueh, H. Y. et al. Positive feedback between PU.1 and the cell cycle controls myeloid differentiation. Science 341, 670–673 (2013).
- Desai, R. V. et al. A DNA-repair pathway can affect transcriptional noise to promote cell fate transitions. Science 373, eabc6506 (2021).
- Galloway, K. E., Franco, E. & Smolke, C. D. Dynamically reshaping signaling networks to program cell fate via genetic controllers. Science 341, 1235005 (2013).
- Chen, J.-Y. et al. Multi-range ERK responses shape the proliferative trajectory of single cells following oncogene induction. *Cell Rep.* 42, 112252 (2023).
- Takahashi, K. & Yamanaka, S. Induction of pluripotent stem cells from mouse embryonic and adult fibroblast cultures by defined factors. Cell 126, 663–676 (2006).
- Hong, M., Clubb, J. D. & Chen, Y. Y. Engineering CAR-T cells for next-generation cancer therapy. Cancer Cell 38, 473–488 (2020).
- Goglia, A. G. et al. A live-cell screen for altered Erk dynamics reveals principles of proliferative control. Cell Syst. 10, 240–253 (2020).
- Li, H.-S. et al. Multidimensional control of therapeutic human cell function with synthetic gene circuits. Science 378, 1227–1234 (2022).
- Collins, R. L. et al. A cross-disorder dosage sensitivity map of the human genome. Cell 185, 3041–3055 (2022).
- Arita, Y. et al. A genome-scale yeast library with inducible expression of individual genes. Mol. Syst. Biol. 17, e10207 (2021).
- 13. Chapman, S. A. & Asthagiri, A. R. Quantitative effect of scaffold abundance on signal propagation. *Mol. Syst. Biol.* **5**, 313 (2009).
- Legut, M. et al. A genome-scale screen for synthetic drivers of T cell proliferation. *Nature* 603, 728–735 (2022).
- Eguchi, A. et al. Reprogramming cell fate with a genome-scale library of artificial transcription factors. Proc. Natl Acad. Sci. USA 113, E8257–E8266 (2016).

- Veerapandian, V. et al. Directed evolution of reprogramming factors by cell selection and sequencing. Stem Cell Reports 11, 593–606 (2018).
- Joung, J. et al. A transcription factor atlas of directed differentiation. Cell 186, 209–229 (2023).
- Gao, X. J., Chong, L. S., Kim, M. S. & Elowitz, M. B. Programmable protein circuits in living cells. Science 361, 1252–1258 (2018).
- Zhu, R., del Rio-Salgado, J. M., Garcia-Ojalvo, J. & Elowitz, M. B. Synthetic multistability in mammalian cells. Science 375, eabq9765 (2022).
- Elowitz, M. B. & Leibler, S. A synthetic oscillatory network of transcriptional regulators. *Nature* 403, 335–338 (2000).
- Gardner, T. S., Cantor, C. R. & Collins, J. J. Construction of a genetic toggle switch in *Escherichia coli*. *Nature* 403, 339–342 (2000).
- Danino, T., Mondragón-Palomino, O., Tsimring, L. & Hasty, J. A synchronized quorum of genetic clocks. *Nature* 463, 326–330 (2010).
- 23. Tabor, J. J. et al. A synthetic genetic edge detection program. *Cell* **137**, 1272–1281 (2009).
- Bashor, C. J., Helman, N. C., Yan, S. & Lim, W. A. Using engineered scaffold interactions to reshape MAP kinase pathway signaling dynamics. *Science* 319, 1539–1543 (2008).
- Ravindran, P. T., McFann, S., Thornton, R. H. & Toettcher, J. E. A synthetic gene circuit for imaging-free detection of signaling pulses. Cell Syst. 13, 131–142 (2022).
- Jones, R. D. et al. An endoribonuclease-based feedforward controller for decoupling resource-limited genetic modules in mammalian cells. Nat. Commun. 11, 5690 (2020).
- Qian, Y., Huang, H.-H., Jiménez, J. I. & Del Vecchio, D. Resource competition shapes the response of genetic circuits. ACS Synth. Biol. 6, 1263–1272 (2017).
- 28. Frei, T. et al. Characterization and mitigation of gene expression burden in mammalian cells. *Nat. Commun.* **11**, 4641 (2020).
- Ceroni, F. et al. Burden-driven feedback control of gene expression. Nat. Methods 15, 387–393 (2018).
- Di Blasi, R. et al. Resource-aware construct design in mammalian cells. Nat. Commun. 14, 3576 (2023).
- Cabrera, A. et al. The sound of silence: transgene silencing in mammalian cell engineering. Cell Syst. 13, 950–973 (2022).
- 32. Duran, A. G. et al. Limiting transactivator amounts contribute to transgene mosaicism in Tet-On all-in-one systems. *ACS Synth. Biol.* **11**, 2623–2635 (2022).
- 33. Heinz, N., Hennig, K. & Loew, R. Graded or threshold response of the tet-controlled gene expression: all depends on the concentration of the transactivator. *BMC Biotechnol* **13**, 5 (2013).
- 34. Khalil, A. S. et al. A synthetic biology framework for programming eukaryotic transcription functions. *Cell* **150**, 647–658 (2012).
- Donahue, P. S. et al. The COMET toolkit for composing customizable genetic programs in mammalian cells. *Nat. Commun.* 11, 779 (2020).
- Wu, M.-R. et al. A high-throughput screening and computation platform for identifying synthetic promoters with enhanced cell-state specificity (SPECS). Nat. Commun. 10, 2880 (2019).
- Bragdon, M. D. J. et al. Cooperative assembly confers regulatory specificity and long-term genetic circuit stability. *Cell* 186, 3810–3825 (2023).
- 38. Randolph, L. N., Bao, X., Zhou, C. & Lian, X. An all-in-one, Tet-On 3G inducible PiggyBac system for human pluripotent stem cells and derivatives. *Sci. Rep.* **7**, 1549 (2017).
- Nevozhay, D., Zal, T. & Balázsi, G. Transferring a synthetic gene circuit from yeast to mammalian cells. *Nat. Commun.* 4, 1451 (2013).
- 40. Beerli, R. R. & Barbas, C. F. Engineering polydactyl zinc-finger transcription factors. *Nat. Biotechnol.* **20**, 135–141 (2002).

- Jamieson, A. C., Kim, S. H. & Wells, J. A. In vitro selection of zinc fingers with altered DNA-binding specificity. *Biochemistry* 33, 5689–5695 (1994).
- 42. Ede, C., Chen, X., Lin, M.-Y. & Chen, Y. Y. Quantitative analyses of core promoters enable precise engineering of regulated gene expression in mammalian cells. ACS Synth. Biol. **5**, 395–404 (2016).
- Zopf, C. J., Quinn, K., Zeidman, J. & Maheshri, N. Cell-cycle dependence of transcription dominates noise in gene expression. PLoS Comput. Biol. 9, e1003161 (2013).
- Quarton, T. et al. Uncoupling gene expression noise along the central dogma using genome engineered human cell lines. Nucleic Acids Res. 48, 9406–9413 (2020).
- Babos, K. N. et al. Mitigating antagonism between transcription and proliferation allows near-deterministic cellular reprogramming. Cell Stem Cell 25, 486–500 (2019).
- 46. Fitzgerald, M., Livingston, M., Gibbs, C. & Deans, T. L. Rosa26 docking sites for investigating genetic circuit silencing in stem cells. *Synth. Biol.* **5**, ysaa014 (2020).
- 47. Jones, R. D. et al. Robust and tunable signal processing in mammalian cells via engineered covalent modification cycles. *Nat. Commun.* **13**, 1720 (2022).
- 48. Frei, T., Chang, C.-H., Filo, M., Arampatzis, A. & Khammash, M. A genetic mammalian proportional-integral feedback control circuit for robust and precise gene regulation. *Proc. Natl Acad. Sci. USA* **119**, e2122132119 (2022).
- Johnstone, C. P. & Galloway, K. E. Supercoiling-mediated feedback rapidly couples and tunes transcription. Cell Rep. 41, 111492 (2022).
- Lillacci, G., Benenson, Y. & Khammash, M. Synthetic control systems for high performance gene expression in mammalian cells. Nucleic Acids Res. 46, 9855–9863 (2018).
- Strovas, T. J., Rosenberg, A. B., Kuypers, B. E., Muscat, R. A. & Seelig, G. MicroRNA-based single-gene circuits buffer protein synthesis rates against perturbations. ACS Synth. Biol. 3, 324–331 (2014).
- Peterman, E. L. et al. High-resolution profiling reveals coupled transcriptional and translational regulation of transgenes. *Nucleic Acids Res.* 53, gkaf528 (2025).
- Askary, A. et al. In situ readout of DNA barcodes and single base edits facilitated by in vitro transcription. *Nat. Biotechnol.* 38, 66–75 (2020).
- Kim, T., Weinberg, B., Wong, W. & Lu, T. K. Scalable recombinase-based gene expression cascades. *Nat. Commun.* 12, 2711 (2021).
- Loveless, T. B. et al. Lineage tracing and analog recording in mammalian cells by single-site DNA writing. *Nat. Chem. Biol.* 17, 739–747 (2021).
- Sheth, R. U. & Wang, H. H. DNA-based memory devices for recording cellular events. Nat. Rev. Genet. 19, 718–732 (2018).
- Shi, D., Toyonaga, S. & Anderson, D. G. In vivo RNA delivery to hematopoietic stem and progenitor cells via targeted lipid nanoparticles. *Nano Lett.* 23, 2938–2944 (2023).
- Sago, C. D. et al. High-throughput in vivo screen of functional mRNA delivery identifies nanoparticles for endothelial cell gene editing. Proc. Natl Acad. Sci. USA 115, E9944–E9952 (2018).
- Blanch-Asensio, A. et al. STRAIGHT-IN enables high-throughput targeting of large DNA payloads in human pluripotent stem cells. Cell Rep. Methods 2, 100300 (2022).
- Weinberg, B. H. et al. High-performance chemical- and light-inducible recombinases in mammalian cells and mice. *Nat. Commun.* 10, 4845 (2019).
- Lende-Dorn, B. A., Atkinson, J. C., Bae, Y. & Galloway, K. E. Chemogenetic tuning reveals optimal MAPK signaling for cell-fate programming. *Cell Rep.* 44, 116226 (2025).

- 62. Ilia, K. et al. Synthetic genetic circuits to uncover the OCT4 trajectories of successful reprogramming of human fibroblasts. *Sci. Adv.* **9**, eadg8495 (2023).
- 63. Velychko, S. et al. Excluding Oct4 from Yamanaka cocktail unleashes the developmental potential of iPSCs. *Cell Stem Cell* **25**, 737–753 (2019).
- Hu, X. et al. Reprogramming progressive cells display low CAG promoter activity. Stem Cells 39, 43–54 (2021).
- 65. Okada, M. & Yoneda, Y. The timing of retroviral silencing correlates with the quality of induced pluripotent stem cell lines. *Biochim. Biophys. Acta* **1810**, 226–235 (2011).
- Wang, N. B. et al. Compact transcription factor cassettes generate functional, engraftable motor neurons by direct conversion. *Cell* Syst. 16, 101206 (2025).
- 67. Beitz, A. et al. Cells transit through a quiescent-like state to convert to neurons at high rates. Preprint at *bioRxiv* https://doi.org/10.1101/2024.11.22.624928 (2024).
- 68. Du, R., Flynn, M. J., Honsa, M., Jungmann, R. & Elowitz, M. B. miRNA circuit modules for precise, tunable control of gene expression. Preprint at *bioRxiv* https://doi.org/10.1101/2024.03.12.583048 (2024).
- Flynn, M. J., Mayfield, A. M., Du, R., Gradinaru, V. & Elowitz, M. B. Synthetic dosage-compensating miRNA circuits for quantitative gene therapy. Preprint at *bioRxiv* https://doi.org/ 10.1101/2024.03.13.584179 (2024).
- Bashor, C. J., Hilton, I. B., Bandukwala, H., Smith, D. M. & Veiseh, O. Engineering the next generation of cell-based therapeutics. *Nat. Rev. Drug Discov.* 21, 655–675 (2022).
- Rai, K. et al. Ultra-high throughput mapping of genetic design space. Preprint at bioRxiv https://doi. org/10.1101/2023.03.16.532704 (2025).
- Tycko, J. et al. High-throughput discovery and characterization of human transcriptional effectors. Cell 183, 2020–2035.e16 (2020).
- 73. Ravindran, P. T., Wilson, M. Z., Jena, S. G. & Toettcher, J. E. Engineering combinatorial and dynamic decoders using synthetic immediate-early genes. *Commun. Biol.* **3**, 436 (2020).
- Hong, C. K. Y. & Cohen, B. A. Genomic environments scale the activities of diverse core promoters. *Genome Res.* 32, 85–96 (2022).
- Johnstone, C. P., Wang, N. B., Sevier, S. A. & Galloway, K. E. Understanding and engineering chromatin as a dynamical system across length and timescales. *Cell Syst.* 11, 424–448 (2020).
- Bartman, C. R., Hsu, S. C., Hsiung, C. C.-S., Raj, A. & Blobel, G. A. Enhancer regulation of transcriptional bursting parameters revealed by forced chromatin looping. *Mol. Cell* 62, 237–247 (2016).
- 77. Popp, A. P., Hettich, J. & Gebhardt, J. C. M. Altering transcription factor binding reveals comprehensive transcriptional kinetics of a basic gene. *Nucleic Acids Res.* **49**, 6249–6266 (2021).
- 78. Weinberg, B. H. et al. Large-scale design of robust genetic circuits with multiple inputs and outputs for mammalian cells. *Nat. Biotechnol.* **35**, 453–462 (2017).
- 79. Short, A. E., Kim, D., Milner, P. T. & Wilson, C. J. Next generation synthetic memory via intercepting recombinase function. *Nat. Commun.* **14**, 5255 (2023).
- 80. Meinke, G., Bohm, A., Hauber, J., Pisabarro, M. T. & Buchholz, F. Cre recombinase and other tyrosine recombinases. *Chem. Rev.* **116**, 12785–12820 (2016).
- 81. Shen, Y. et al. SCRaMbLE generates designed combinatorial stochastic diversity in synthetic chromosomes. *Genome Res.* **26**, 36–49 (2016).
- 82. Liu, W. et al. Rapid pathway prototyping and engineering using in vitro and in vivo synthetic genome SCRaMbLE-in methods. *Nat. Commun.* **9**, 1936 (2018).

- Koeppel, J. et al. Randomizing the human genome by engineering recombination between repeat elements. Science 387, eado3979 (2025).
- Pinglay, S. et al. Multiplex generation and single-cell analysis of structural variants in mammalian genomes. Science 387, eado5978 (2025).
- Cautereels, C. et al. Combinatorial optimization of gene expression through recombinase-mediated promoter and terminator shuffling in yeast. Nat. Commun. 15, 1112 (2024).
- 86. Chakravarti, D., Caraballo, L. D., Weinberg, B. H. & Wong, W. W. Inducible gene switches with memory in human T cells for cellular immunotherapy. ACS Synth. Biol. 8, 1744–1754 (2019).
- Durrant, M. G. et al. Systematic discovery of recombinases for efficient integration of large DNA sequences into the human genome. *Nat. Biotechnol.* 41, 488–499 (2023).
- Jelicic, M. et al. Discovery and characterization of novel Cre-type tyrosine site-specific recombinases for advanced genome engineering. *Nucleic Acids Res.* 51, 5285–5297 (2023).
- 89. Kretzschmar, K. & Watt, F. M. Lineage tracing. Cell 148, 33-45 (2012).
- Yang, D. et al. Lineage tracing reveals the phylodynamics, plasticity, and paths of tumor evolution. Cell 185, 1905–1923 (2022).
- Anderson, T. et al. Ligament injury in adult zebrafish triggers ECM remodeling and cell dedifferentiation for scar-free regeneration. NPJ Regen. Med. 8, 51 (2023).
- 92. Nowak, J. A., Polak, L., Pasolli, H. A. & Fuchs, E. Hair follicle stem cells are specified and function in early skin morphogenesis. *Cell Stem Cell* **3**, 33–43 (2008).
- 93. Le Bin, G. C. et al. Oct4 is required for lineage priming in the developing inner cell mass of the mouse blastocyst. *Development* **141**, 1001–1010 (2014).

- 94. Meador, K. et al. Achieving tight control of a photoactivatable Cre recombinase gene switch: new design strategies and functional characterization in mammalian cells and rodent. *Nucleic Acids Res.* **47**, e97 (2019).
- 95. Bleris, L. et al. Synthetic incoherent feedforward circuits show adaptation to the amount of their genetic template. *Mol. Syst. Biol.* **7**, 519 (2011).
- Yang, J. et al. A synthetic circuit for buffering gene dosage variation between individual mammalian cells. *Nat. Commun.* 12, 4132 (2021).
- Love, K. S. et al. Model-guided design of microRNA-based gene circuits supports precise dosage of transgenic cargoes into diverse primary cells. Cell Syst. 16, 101269 (2025).
- An, M. et al. Engineered virus-like particles for transient delivery of prime editor ribonucleoprotein complexes in vivo. Nat. Biotechnol. 42, 1526–1537 (2024).
- 99. Kreitz, J. et al. Programmable protein delivery with a bacterial contractile injection system. *Nature* **616**, 357–364 (2023).

Publisher's note Springer Nature remains neutral with regard to jurisdictional claims in published maps and institutional affiliations.

Springer Nature or its licensor (e.g. a society or other partner) holds exclusive rights to this article under a publishing agreement with the author(s) or other rightsholder(s); author self-archiving of the accepted manuscript version of this article is solely governed by the terms of such publishing agreement and applicable law.

© The Author(s), under exclusive licence to Springer Nature America, Inc. 2025

Methods

Experimental model

Cell lines and tissue culture. Human: HEK293T ATCC cat. no. CRL-3216; human: Plat-E Retroviral Packaging Cell Line Cell Biolabs cat. no. RV-101; human: iPSC Line (Episomal, HFF) ALSTEM cat. no. iPS11; mouse: B6.Cg-Tg(Hlxb9-GFP)1Tmj/J The Jackson Laboratory cat. no. 005029, RRID:IMSR_JAX:005029 (sex was not tested for; primary MEFs isolated for this study were isolated from embryos of both sexes). HEK293T cells, Plat-E cells and MEFs were cultured using DMEM (Genesee Scientific, cat. no. 25-500) + 10% FBS (Genesee Scientific, cat. no. 25-514H). Plat-E cells were selected using 10 ug ml⁻¹ blastocidin and 1 µg ml⁻¹ puromycin every three passages. IPS11 cells were cultured using mTeSR Plus (STEMCELL Technologies, cat. no. 100-1130) with Geltrex (ThermoFisher Scientific, cat. no. A1413302) coating. HEK293T cells, Plate-E cells and MEFs were detached from flasks using Trypsin (Genesee Scientific, cat. no. 25-510) diluted in PBS. For experiments, iPS11 cells were dissociated into single cells using Gentle Cell Dissociation Reagent (STEMCELL Technologies, cat. no. 100-1077) and replated in mTeSR Plus with ROCK inhibitor (Millipore Sigma, cat. no. Y0503-5MG) and Penicillin-Streptomycin (ThermoFisher Scientific, cat. no. 10-378-016). All cells were incubated at 37 °C with 5% CO₂ and periodically tested for mycoplasma.

Primary MEF dissection and isolation. C57BL/6 mice were mated with mice bearing the Hb9::GFP reporter (B6.Cg-Tg(Hlxb9-GFP)1Tmj/J). Mice were housed in a 12-h light/12-h dark cycle with ambient temperature and humidity and with access to food and water. MEFs with (for conversion experiments) or without Hb9::GFP reporter (for nonconversion experiments) of both sexes were isolated at embryonic day 12.5–14.5 under a dissection microscope as described previously^{61,66}. Embryos were sorted into nontransgenic and Hb9::GFP+ by using a blue laser on spinal tissue to identify the presence of Hb9::GFP+ cells. Passage 1 MEFs were tested for mycoplasma, cryopreserved in 90% FBS and 10% DMSO, and stored in liquid nitrogen. All cells were incubated at 37 °C with 5% CO₂.

Method details

Plasmid cloning. Plasmids were cloned using standard protocols for Gibson assembly and Golden Gate assembly. Promoters, target genes and polyA signals were inserted into part position vectors (pPVs) via Gibson assembly or Golden Gate assembly. Expression plasmids were assembled via Bsal (New England Biolabs, cat. no. R3733L) Golden Gate assembly using pPVs or Q5 polymerase-amplified and gel-purified DNA fragments. The lentivirus or retrovirus plasmids were assembled with PaqCl (New England Biolabs, cat. no. R0745L) Golden Gate assembly or Gateway assembly using expression plasmids and viral backbone plasmids. Key novel expression plasmids for transfection and viral production are provided in the Supplementary Information and at Addgene.

DIAL and TET-DIAL promoter cloning. The DIAL promoter was constructed by inserting putatively neutral spacer sequence(s) between loxP or VloxP sites, and subsequently between ZF binding sites and a YB TATA minimal promoter. The loxP and VloxP sequences were taken from recombinase reporters (gifts from the Wong Lab at Boston University, BW338 and BW273). Tessellated ZF43/37 hybrid binding sites were taken from ZF reporter Addgene no. 138934. The DIAL promoter was assembled through subsequent Gibson assembly and Esp3I/PaqCI (New England Biolabs, cat. nos. R0734S and R0745L) Golden Gate assembly with oligonucleotides or PCR products of spacer sequence, ZF binding sites, minimal promoter and recombinase sites with complementary overhangs. Different minimal promoter oligomers were inserted through Bsal Golden Gate with PCR fragments or pPVs of the other promoter components. The TET-DIAL promoter was constructed by inserting a putatively neutral spacer sequence between loxP or VloxP sites, tetO sites and various minimal promoters in a similar manner

to DIAL promoter cloning. TetO binding sites were amplified from TRE-dCas9-VPR Addgene plasmid no. 63800. The assembled DIAL and TET-DIAL promoters were cloned into expression or viral vectors with target genes and polyA signals for transfection or transduction via Golden Gate. Sequences are available in the Supplementary Information. Unless specified, the minimal promoter was YB TATA.

Recombinase and ZFa plasmids and cloning. Unless otherwise specified, in transient transfections, recombinase was expressed as: Cre from pCAG-iCre (Addgene plasmid no. 89573), VCre from pCAG-VCre (Addgene plasmid no. 89575), GIB-Cre N-terminal (Addgene plasmid no. 108723) and GIB-Cre C-terminal (Addgene plasmid no. 108724) (gifts from Wilson Wong at Boston University). modRNA for iCre is produced from Addgene no. 232773 and modRNA for eeBxb1 is from Addgene no. 232748. The PuroR-2A-iCre, mRuby2-2A-PuroR and TagBFP were cloned into vectors for modRNA production with Gibson assembly. The Cre variants were cloned with Gibson and Gateway assembly into retrovirus backbones for delivery to MEFs. ZFa sequences were: CMV-VP64-ZF37-BGH (Addgene no. 138834), CMV-VP64-ZF43-BGH (Addgene no. 138835) and CMV-VPR-ZF37-BGH (Addgene no. 138839). PCR fragments of Addgene plasmids no. 138759 and no. 138730 were used to clone target gene pPVs for VP16-ZF37 and VP16-ZF43 with 2A-fluorescent proteins through Gibson assembly. The 2A-tagged ZFs were subsequently inserted into expression vectors with promoters and poly A signal via Bsal Golden Gate assembly, and subsequently into viral backbones with PagCI Golden Gate assembly or Gateway assembly. Unless specified, VP16-ZF43 and VP16-ZF37 are expressed from EF1a promoter with BGH polyA in expression and lentivirus constructs. All plasmids for transient transfection contained BGH. Sequences are available in the Supplementary Information.

HEK293T DNA transient transfection experiments. Cell were plated 24 h before HEK293T transfections (39,000-42,000 cells per 96-well plate, 390,000-420,000 cells per 12-well plate or 1,150,000-1,300,000 cells per 6-well plate). Cells were transfected on day 0 via a 4:1 ratio of μg of PEI to μg of DNA mixed in KnockOut DMEM (Fisher Scientific, cat. no. 10-829-018). DNA amounts are detailed in Supplementary Table 1. Unless specified, at the 96-well scale, each well was transfected with 112.5 ng of all plasmids except the recombinase plasmid (11 ng per well), including a co-transfection marker (EF1a-iRFP670-SV40, 112.5 ng). An empty vector was used to keep total DNA and PEI consistent. At 1 dpt. medium was aspirated and replaced with DMEM + 10% FBS. When specified in figure captions, small molecules and modRNA were added at 1 dpt. Cells were flowed and imaged at 3 dpt in technical triplicates. $Bioreplicates\ represent\ separate\ transfection\ experiments.\ To\ detach$ cells from wells in preparation for flow cytometry or immunostaining, a 1:1 Trypsin/1 × PBS mixture was added to each well. After 8 min, DMEM + 10% FBS was added on top. For 96-well plates, cells were centrifuged in plates at 1,000g for 10 min. For 12-well plates or 6-well plates, cells were centrifuged in tubes at 400g for 5 min and processed with RNA-FISH or immunofluorescent staining when specified. For flow cytometry, cells were resuspended in PBS. Unless specified, transfection refers to transient transfection of plasmid DNA and cells were gated based on co-transfection marker.

HCR Flow RNA-FISH. In all HCR Flow RNA-FISH (hybridization chain reaction RNA-FISH with flow cytometry) experiments here, we use the Molecular Instruments probe set for mGL compatible with B1 amplifiers conjugated to Alexa Fluor 647. The FISH protocol was previously optimized for flow cytometry⁵², and the protocol was based on those reported in ref. 100 and ref. 101. All buffer compositions are detailed in ref. 52. Briefly, HEK293T cells were transfected with plasmids at the 12-well scale. At 3 dpt, cells were dissociated, spun, fixed, permeabilized and probed as previously described in ref. 52. In analysis, cells were gated based on co-transfection marker mRuby2.

Western blot. We plated 1.2 million HEK293T cells at a 6-well plate scale 24 h before transfection. Cells were transfected with EF1a-Flag-VP16-ZF37-2A-mCherry-BGH, EF1a-Flag-VP16-ZF43-2A-TagBFP-BGH, CAG-3xFlag-iRFP670-BGH and N- and C-terminal split GIB-Cre according to Supplementary Table 1 and figure captions. At 3 dpt, cells were washed with cold PBS and placed on ice, and scraped with 67 µl of RIPA buffer (Cell Signaling Technology, cat. no. 9806) and 1 mM PMSF (Cell Signaling Technology, cat. no. 8553) for 5 min. Cells were further sheared using a 21-gauge blunt needle. The cell lysate was spun down at 14,000g for 15 min at 4 °C. Samples were separated using electrophoresis in 4–15% Mini-PROTEAN TGX (Bio-Rad, cat. no. 4561086) precast gels or 15% hand-poured bis-tris gels. We loaded 10 μg of total cell protein per well. Proteins were transferred to a PVDF membrane using the iBLOT 2 Dry Blotting System. Membranes were blocked with blocking buffer (5% milk and 0.1% Tween-20 in PBS) for 1 h at room temperature, and incubated overnight at 4 °C with primary antibody. Cells were washed three times and incubated with HRP-conjugated secondary antibodies in blocking buffer. Membranes were then washed five times before HRP signal detection via SuperSignal West Femto Maximum Sensitivity Substrate (Thermo Scientific, cat. no. 34096). The primary antibodies used in this western blot were: mouse anti β-actin (8H10D10) (1:50,000 dilution, Cell Signaling Technology, cat. no. 3700, AB 2242334); mouse monoclonal anti-Flag M2 (1:20,000 dilution, Sigma-Aldrich, cat. no. F1804, RRID:AB_262044). The secondary antibodies used in this western blot were: goat anti-mouse IgG H&L (HRP) (1:50,000 dilution, Abcam, cat. no. ab205719, RRID:AB 2755049); goat anti-rabbit IgG H&L (HRP) (1:50,000 dilution, Abcam, cat. no. ab6721, RRID:AB_955447).

Immunofluorescent staining for flow (flow staining). HEK293T cells were transfected with plasmids at the 12-well plate scale according to Supplementary Table 1. At 3 dpt, cells were detached as described for HEK293T DNA transient transfection. Cells were fixed with 3.7% paraformaldehyde, permeabilized and resuspended with primary antibody in blocking solution (5% FBS, 0.1% Tween in PBS) overnight. The next day, cells were washed with 3% FBS in 1 × PBS and centrifuged. Cells were resuspended with secondary antibody in blocking solution (5% FBS, 0.1% Tween in PBS) for 30 min. Cells were then washed, centrifuged and resuspended in PBS for flow cytometry. Centrifugation was at 400g. In analysis, cells were gated based on a co-transfection marker, iRFP670. The primary antibodies were: mouse monoclonal anti-Flag M2 (1:400 dilution, Sigma-Aldrich, cat. no. F3165, RRID:AB 259529). The secondary antibodies were: goat anti-Mouse IgG (H+L) Cross-Adsorbed Secondary Antibody, Alexa Fluor 555 (1:400 dilution, Thermo Fisher Scientific, cat. no. A-21422, RRID:AB 2535844).

iPSC transient transfection experiments. At 48 h before transfection, 15,000 iPS11 cells were plated per well in a 96-well plate with media containing ROCK inhibitor. At 24 h before transfection, the media containing ROCK inhibitor was removed. On the day of transfection, the medium was changed to Opti-MEM (ThermoFisher Scientific, cat. no. 31985062) and transfection mixes were prepared with FUGENE HD (FuGENE, cat. no. HD-1000) according to the manufacturer's instructions (ratio of 3 μ l of reagent to 1 μ g of DNA). At 4 h after transfection, mTeSR Plus with Penicillin-Streptomycin was added. At 24 h after transfection, the medium was changed to mTeSR Plus with Penicillin-Streptomycin and, if specified, DOX (1 μ g ml $^{-1}$). Cells were dissociated and resuspended in 1 × PBS and transferred to a round-bottomed plate for flow cytometry. Transfection DNA amounts are detailed in Supplementary Table 1. Cells were gated on co-transfection marker TagBFP with additional gating as specified.

PCR of cell lysis. DNA from transfected HEK293T cells was extracted with Cell Lysis Buffer ($10\times$) (Cell Signaling Technology, cat. no. 9803S). Cells were dissociated, pelleted and resuspended in 50 μ l of Cell Lysis

Buffer (10×) and 0.5 μ l of Proteinase K (New England Biolabs, cat. no. P8107S) per sample. Cells were incubated for 45 min at 85 °C. Then, 1 μ l of the supernatant was used for PCR using Apex Taq RED Master Mix, 2× (Genesee Scientific, cat. no. 42-138B). Supplementary Figs. 4b,d and 18f useprimers/S'-ACCACCCCGGTGAACAGCTC-3')and(5'-CGCCCGGAGCCGATTTGAAC-3'). Supplementary Fig. 4g uses primers (5'-ACCACCCCGGTGAACAGCTC-3') and (5'-TGTTCGTACTCGGATCGGGAGATCTG-3'). PCR products were run on a 2% agarose gel at 110 V for 45–60 min.

Retrovirus production in Plat-E cells. Plat-E cells were seeded at 850,000 per 6-well plate, onto plates coated with 0.1% gelatin. The next day, Plat-E cells were transfected with 1.8 µg of DNA per well using a 4:1 ratio of µg PEI:µg DNA. The next day, the medium was replaced with 1.25 ml of fresh 25 mM HEPES-buffered DMEM with 10% FBS. Filtered viral supernatant was then used for transduction of MEFs.

Lentiviral production in HEK293T cells. HEK293T cells were seeded at 1 million per 6-well plate, onto plates coated with 0.1% gelatin. The next day, each well of 293T cells was transfected with 1.02 μg of packaging plasmid (psPax2, Addgene no. 12260), 2.05 μg of envelope plasmid (pMD2.G, Addgene no. 12259) and 1.02 μg of transfer plasmid using a 4:1 ratio of μg of PEI: μg of DNA. After 6–8 h, the medium was replaced with 1.25 ml of fresh 25 mM HEPES-buffered DMEM with 10% FBS. Two collections of virus were made, at 24 and 48 h. Virus was filtered, then incubated with Lenti-X concentrator overnight. The virus was pelleted by centrifugation at 1,500g for 45 min at 4 °C. The supernatant was removed, and the pellets were resuspended in medium to a final volume of 33 μ l per 6-well plate of virus. Volumes and cell numbers were scaled up proportionally for a 10-cm plate and resuspended in a final volume of 200 μ l.

Viral transduction of MEFs with mGL DIAL reporter. MEFs were seeded 1 day before viral transduction onto plates coated with 0.1% gelatin, at 10,000 per 96-well plate. MEFs were transduced 2 days in a row with 11 μ l of each Plat-E retrovirus per 96-well plate. On the second day, MEFs were also transduced with 3 μ l per 96-well plate of concentrated lentivirus from a 6-well plate, or 5 μ l per 96-well plate of concentrated lentivirus from a 10-cm plate. At 3–4 dpi, the cells were dissociated using trypsin and analyzed via flow cytometry.

Conversion of MEFs to iMNs using DIAL and TET-DIAL. MEFs were seeded at 5,000 per 96-well plate, onto plates that had been coated with 0.1% gelatin. At -1 dpi, MEFs were transduced with retrovirus of conversion factors (Lhx3-Ngn2-Isl1, Addgene no. 233195) and SNAP-p53DD (Addgene no. 244168) as described previously^{61,66}. Conditions with GIB-inducible Cre additionally received retroviruses with the N-terminal and C-terminal split GIB-Cre. Cells were spinfected at 1,500g for 30 min. The next day (0 dpi), MEFs were spinfected with lentiviruses at 1,500g for 30 min. For DIAL, the lentiviruses used were 2.5 μl of PGK-VP16-ZF37-2A-TagBFP-WPRE (+ZFa conditions), 4 μl of a 380-bp spacer DIAL promoter driving mCherry-HRas^{G12V}-BGH with divergent EF1a-SNAP-WPRE or 4 µl of a no-spacer control DIAL pro $moter\ driving\ mCherry-HRas^{G12V}-WPRE.\ For\ TET-DIAL, the\ lentiviruses$ used were 4 µl of a 380-bp spacer TET-DIAL promoter driving mCherry-HRas^{G12V}-BGH, or 4 μl of no-spacer control TET-DIAL promoter driving mCherry-HRas^{G12V}-bGH, both with a divergent EFS-rtTA-TagBFP-WPRE. Conditions without lentivirus were given fresh media. For proliferation measurements, cells were stained with CellTrace Far Red (CTFR, Thermo Scientific, cat. no. C34564) the day after lentiviral infection $(1 \, dpi)$. Cells were washed with PBS, then incubated with $1 \, \mu M$ CTFR in PBS for 30 min at 37 °C. Then CTFR solution was removed and replaced with fresh media. Conversion conditions assessed at 14 dpi did not undergo CTFR staining and received fresh media. As specified for each condition, media at 1 dpi included GIB (1 µM, maintained up to 5 dpi), DOX (1 µg ml⁻¹, maintained as noted in figures) or 100 ng of modRNA

of eeBxb1 or PuroR-2A-Cre with Lipofectamine for transfection. At 3 dpi, the cells were switched to N3 media, as described previously $^{4-6}$, and refreshed every 2–3 days until assaying. Cell were dissociated with Trypsin and flowed at 5 dpi to evaluate hyperproliferation via flow cytometry. The hyperproliferation gate was defined as the 20% of cells with the lowest CTFR in a control retrovirally Puro-infected condition for each MEF batch. For conversion quantification, cells were dissociated at 14 dpi using DNase/Papain (Worthington Biochemical, cat. no. LK003172/Worthington Biochemical, cat. no. LK003178) dissociation system and analyzed via flow cytometry. iMNs were identified as bright Hb9::GFP-positive cells.

In vitro transcription and transfection of modRNA. The plasmid template used for Cre. TagBFP, eeBxb1, PuroR-2A-Cre and mRuby2-2A-PuroR modRNA synthesis harbors the 5' untranslated region (UTR) of human β-globin, a Kozak sequence, the coding sequence and the 3' UTR of human β-globin. The linear template for in vitro transcription was generated via PCR using Q5 DNA Polymerase (New England Biolabs) with the forward primer (5'-AGCTATAATACGACTCACTATAAGctcctgggcaacgtgctg-3') encoding the T7 promoter (upper-case bases) and binding the 5′ UTR (lower-case bases) and the reverse primer (5'-poly(T)₁₁₆-GCAATGAAAATAAATG TTTTTTATTAGGCAGAAT-3') encoding the poly(A) tail and binding the 3' UTR. The PCR product was isolated on a 1% agarose gel, excised and purified using the Monarch PCR and DNA Cleanup Kit (New England Biolabs). Then, 200 ng of purified product was used in a 20-µl in vitro transcription reaction with HiScribe T7 High Yield RNA Synthesis Kit (New England Biolabs), fully substituting UTP with N1-methylpseudouridine-5'-phosphate (TriLink Biotechnologies) and co-transcriptionally capping with CleanCap Reagent AG (TriLink Biotechnologies). modRNA was stored at -80 °C. Transfections were performed according to the manufacturer's instructions with 0.2 µl of Lipofectamine MessengerMAX (Thermo Fisher Scientific) per 100 ng of modRNA.

Viral transduction of HEK293T cells and cell line development with mGL DIAL reporter. HEK293T cells were seeded on the day of viral transduction in suspension at 20,000 cells per 96-well plate. Each 96-well plate was transduced with 3 μl per concentrated lentivirus from a 6-well plate, or, when specified, at low multiplicity of infection for single copy integration. Fresh DMEM with 10% FBS was included with 5 μg ml⁻¹ polybrene to increase transduction efficiency. Cells were expanded to the 6-well scale. Integrated lentivirus components included mGL regulated by the 203-bp DIAL promoter with or without divergent EF1a-iRFP670-WPRE as well as ZFa (EF1a-VP16-ZF37-2A-tagBFP-BGH or EF1a-VP16-ZF37-2A-mCherry-BGH), as indicated. At 10 dpt, cells positive for infected components were sorted using a Sony MA900. Post-sort polyclonal cell lines were cultured until confluent and passaged for downstream experiments.

Time-course and inheritability evaluation with modRNA transfection in HEK293T cells. From sorted, polyclonal HEK293T cell lines with virally integrated components and DIAL reporter, 20,000 cells were plated per well into 96-well plates. The next day, cells in +Cre conditions were co-transfected with 100 ng each of Cre and fluorescent marker modRNA. For the time-course experiments, cells were not passaged. For the inheritability experiments, cells were passaged at a 1:5 ratio as indicated. Flow data were gated as indicated in figure captions.

Imaging. Images were taken on a Keyence All-in-one fluorescence microscope, BZ-X800.

Flow cytometry. Flow cytometry was performed with an Attune NxT Acoustic Focusing Cytometer and gated as described in Supplementary Figs. 1c and 2.

Mathematical modeling of DIAL activity for varying levels of 7Fa

Dose-dependent reporter gene activation via ZFa titration was modeled using the Hill equation.

$$\frac{d\left[\text{Reporter}_{\text{RNA}}\right]}{dt} = k_{\text{cat}} \frac{\left[ZF_{protein}\right]^n}{K_M + \left[ZF_{protein}\right]^n} + \alpha - \beta \left[\text{Reporter}_{\text{RNA}}\right]$$

The relationship between reporter gene transcription and translation was simplified to obtain

$$\frac{d\left[\text{Reporter}_{\text{protein}}\right]}{dt} = k_{\text{cat}} \frac{\left[ZF_{\text{protein}}\right]^n}{K_M + \left[ZF_{\text{protein}}\right]^n} + \alpha - \beta \left[\text{Reporter}_{\text{protein}}\right]$$

where k_{cat} is the expression rate constant; α is the leaky expression from TF-independent transcription; and β is the degradation constant.

Assuming steady state of cellular processes, the reporter protein levels are:

[Reporter_{protein}] =
$$\frac{k_{cat}}{\beta} \frac{\left[ZF_{protein}\right]^n}{K_M + \left[ZF_{protein}\right]^n} + \frac{\alpha}{\beta}$$

Experimental data (Fig. 3d and Supplementary Fig. 8b) from the ZFa titration were divided into conditions (for example, in the presence or absence of Cre, VP16-ZF37 titration and VP16-ZF43 titration) to generate separate parameters that capture the different gene regulation processes across pre- and post-excision constructs. Parameters $k_{\rm cat}$, β and α are consolidated to simplify the steady-state equation as follows:

[Reporter_{protein}] =
$$k'_{\text{cat}} \frac{\left[ZF_{protein}\right]^n}{K_M + \left[ZF_{protein}\right]^n} + \alpha'$$

The leakiness parameter α' was set to the lowest value of output mGL in each condition corresponding to no ZFa. Assuming no Hill cooperativity for ZF binding (n=1), the experimental data were used as [$ZF_{protein}$] (proxied by fluorescent protein expression, mCherry for VP16-ZF37 and TagBFP for VP16-ZF43) and [Reporter_protein] (mGL) to calculate parameters k'_{cat} and k'_{cat} from the equation.

To minimize technical variance, the ZFa titration data were normalized within each bioreplicate. For fitting, we excluded the highest levels of input ZFa where burden induces a nonmonotonic trend. The data were transformed such that the leaky mCherry or TagBFP expression in conditions with no ZFa was set to zero.

To fit the model, the data were bootstrapped across each condition (for example, in the presence or absence of Cre). The 95% confidence interval of the titration curve was generated by selecting the 2.5th and 97.5th percentile output mGL values for each input mCherry or TagBFP value. The model was overlaid onto experimental data after reversing the transformation for leaky mCherry or TagBFP expression.

Reporting summary

Further information on research design is available in the Nature Portfolio Reporting Summary linked to this article.

Data availability

All experimental data and analyzed data to support the findings of this study have been made publicly available, as of the date of publication, from the Zenodo repository via https://doi.org/10.5281/zenodo.17014280 (ref. 102). Additional information is available from the corresponding author. Plasmid DNA sequences are available in the Supplementary Information or from Addgene. Plasmids not available through Addgene are available from the corresponding author upon request. Source data are provided with this paper.

Code availability

All code for data analysis, modeling and figure generation is publicly available from the GitHub repository via https://github.com/Galloway-LabMIT/Kabaria_Promoter_Editing_DIAL (ref. 103) and via Zenodo at https://doi.org/10.5281/zenodo.17042201 (ref. 104). Any additional information required to reanalyze the data reported in this paper is available from the corresponding author.

References

- 100. Choi, H. M. T. et al. Third-generation in situ hybridization chain reaction: multiplexed, quantitative, sensitive, versatile, robust. Development 145, dev165753 (2018).
- 101. Jia, Z., Dong, Y., Xu, H. & Wang, F. Optimizing the hybridization chain reaction-fluorescence in situ hybridization (HCR-FISH) protocol for detection of microbes in sediments. *Mar. Life Sci. Technol.* 3, 529–541 (2021).
- 102. Kabaria, S. & Galloway, K. E. Data for Kabaria et al "Programmable Promoter Editing for Precise Control of Transgene Expression". Zenodo https://doi.org/10.5281/zenodo.17014280 (2025).
- 103. Kabaria, S. R. et al. Programmable promoter editing for precise control of transgene expression. Source code. GitHub https://github. com/GallowayLabMIT/Kabaria_Promoter_Editing_DIAL (2025).
- 104. Kabaria, S. R. et al. Programmable promoter editing for precise control of transgene expression. *Zenodo* https://doi.org/10.5281/ zenodo.17042201 (2025).

Acknowledgements

Research reported in this manuscript was supported by the National Institute of General Medical Sciences of the National Institutes of Health under award no. R35-GM143033 and by the National Science Foundation under the NSF-CAREER under award no. 2339986. Research was sponsored by the US Army Research Office and accomplished under cooperative agreement no. W911NF-19-2-0026 for the Institute for Collaborative Biotechnologies. S.R.K., B.A.L.-D. and E.L.P. are supported by the National Science Foundation Graduate Research Fellowship Program under grant no. 1745302. M.E.E. is supported by the National Science Foundation Graduate Research Fellowship Program under grant no. 2141064. A.M.B. is supported

by the National Cancer Institute under award no. F99CA284280. We thank the Koch Institute's R. A. Swanson (1969) Biotechnology Center (National Cancer Institute grant no. P30-CA14051) for technical support, specifically the Flow Cytometry Core Facility. We thank C. Johnstone, J. Teves, D. Godavarti and J. Atkinson for their feedback on the development of the manuscript.

Author contributions

S.R.K., Y.B. and K.E.G. conceived and outlined the project. S.R.K., Y.B., M.E.E. and K.E.G. analyzed DIAL and TET-DIAL characterization. E.L.P. performed HCR Flow FISH. A.M.B. and B.A.L.-D. performed lentiviral delivery to primary mouse embryonic fibroblasts and analyzed data. E.L.P. and K.S.L. performed iPSC transfections. B.A.L.-D., Y.B. and M.E.E. performed cell-fate conversion experiments and analyzed data. D.S.P. assisted with experimental design and production of modRNA. S.R.K., Y.B., M.E.E., A.M.B., B.A.L.-D. and K.E.G. wrote the manuscript. K.E.G. supervised the project.

Competing interests

S.R.K., Y.B., M.E.E. and K.E.G. declare that patent applications related to this work have been filed by the Massachusetts Institute of Technology, PCT/US2025/030574 (MIT Case 25874). The other authors declare no competing interests.

Additional information

Supplementary information The online version contains supplementary material available at https://doi.org/10.1038/s41587-025-02854-y.

Correspondence and requests for materials should be addressed to Kate E. Galloway.

Peer review information *Nature Biotechnology* thanks Alexander Vlahos and the other, anonymous, reviewer(s) for their contribution to the peer review of this work.

Reprints and permissions information is available at www.nature.com/reprints.

nature portfolio

Corresponding author(s):	Galloway, Kate
Last updated by author(s):	9/2/2025

Reporting Summary

Nature Portfolio wishes to improve the reproducibility of the work that we publish. This form provides structure for consistency and transparency in reporting. For further information on Nature Portfolio policies, see our Editorial Policies and the Editorial Policy Checklist.

Please do not complete any field with "not applicable" or n/a. Refer to the help text for what text to use if an item is not relevant to your study. For final submission: please carefully check your responses for accuracy; you will not be able to make changes later.

For all statistical analyses, confirm that the following items are present in the figure legend, table legend, main text, or Methods section.

$\overline{}$					
़ .	ta	t۱	C	H١	CC
S.	ιa	u		u	l

n/a	Confirmed
	The exact sample size (n) for each experimental group/condition, given as a discrete number and unit of measurement
	A statement on whether measurements were taken from distinct samples or whether the same sample was measured repeatedly
	The statistical test(s) used AND whether they are one- or two-sided Only common tests should be described solely by name; describe more complex techniques in the Methods section.
\times	A description of all covariates tested
\times	A description of any assumptions or corrections, such as tests of normality and adjustment for multiple comparisons
	A full description of the statistical parameters including central tendency (e.g. means) or other basic estimates (e.g. regression coefficient) AND variation (e.g. standard deviation) or associated estimates of uncertainty (e.g. confidence intervals)
	For null hypothesis testing, the test statistic (e.g. <i>F</i> , <i>t</i> , <i>r</i>) with confidence intervals, effect sizes, degrees of freedom and <i>P</i> value noted <i>Give P values as exact values whenever suitable.</i>
\times	For Bayesian analysis, information on the choice of priors and Markov chain Monte Carlo settings
\times	For hierarchical and complex designs, identification of the appropriate level for tests and full reporting of outcomes
\times	Estimates of effect sizes (e.g. Cohen's <i>d</i> , Pearson's <i>r</i>), indicating how they were calculated
	Our web collection on statistics for biologists contains articles on many of the points above.

Software and code

Policy information about availability of computer code

Data analysis

Data collection

Attune software was used to collect flow cytometry data.

Cytometry data was analyzed using:
Python 3.9.1Python Software Foundation https://www.python.org; RRID:SCR_008394
FlowJo v10 BD https://www.flowjo.com/solutions/flowjo; RRID:SCR_008520

The following python packages were used for data analysis: fonttools==4.34.4

idna==2.10 imagesize==1.2.0 importlib-metadata==4.10.1 ipykernel==5.4.3 ipython==7.19.0 ipython-genutils==0.2.0 ipywidgets==7.6.3 jedi==0.18.0 Jinja2==2.11.3 json5==0.9.5

jsonschema==3.2.0 jupyter==1.0.0

jupyter-client==6.1.11 jupyter-console==6.2.0

ī

jupyter-core==4.7.0 jupyter-server==1.2.1 jupyterlab==3.0.4 jupyterlab-pygments==0.1.2 jupyterlab-server==2.1.2 jupyterlab-widgets==1.0.0 kfm==1.0.4 kiwisolver==1.3.1 MarkupSafe==1.1.1 matplotlib==3.5.2 matplotlib-inline==0.1.3 mistune==0.8.4 nb-clean==2.0.2 nbclassic==0.2.6 nbclient==0.5.1 nbconvert==6.0.7 nbformat==5.0.8 nest-asyncio==1.4.3 notebook==6.2.0 numpy==1.21.6 openpyxl==3.1.5 packaging==20.9 pandas==1.3.5 pandocfilters==1.4.3 parso==0.8.1 pickleshare==0.7.5 Pillow==9.1.1 prometheus-client==0.9.0 prompt-toolkit==3.0.10 pycparser==2.20 pydantic==1.8.2 pygls==0.11.3 Pygments==2.8.1 pyparsing==2.4.7 pyrsistent==0.17.3 pyspellchecker==0.7.1 python-dateutil==2.8.2 pytz==2021.1 pywin32==300 pywinpty==0.5.7 PyYAML==6.0 pyzmq==23.2.0 qtconsole==5.0.1 QtPy = 1.9.0requests==2.25.1 rushd==0.5.1 scipy==1.7.3 seaborn==0.11.2 Send2Trash==1.5.0 six==1.16.0 sniffio==1.2.0 snowballstemmer==2.1.0 Sphinx==5.0.2sphinx-last-updated-by-git==0.3.0 sphinx-rtd-theme==0.5.1 sphinxcontrib-applehelp==1.0.2 sphinxcontrib-devhelp==1.0.2 sphinxcontrib-htmlhelp==2.0.0 sphinxcontrib-jsmath==1.0.1 sphinxcontrib-qthelp==1.0.3 sphinxcontrib-serializinghtml==1.1.5 statannot==0.2.3 statannotations==0.5.0 terminado==0.9.2 testpath==0.4.4 tornado==6.1 traitlets==5.3.0 typeguard==2.13.3 typing-extensions==4.0.1 urllib3==1.26.5 wcwidth==0.2.5 webencodings==0.5.1 widgetsnbextension==3.5.1 zipp==3.7.0

For manuscripts utilizing custom algorithms or software that are central to the research but not yet described in published literature, software must be made available to editors and reviewers. We strongly encourage code deposition in a community repository (e.g. GitHub). See the Nature Portfolio guidelines for submitting code & software for further information.

Data

Policy information about availability of data

All manuscripts must include a data availability statement. This statement should provide the following information, where applicable:

- Accession codes, unique identifiers, or web links for publicly available datasets
- A description of any restrictions on data availability
- For clinical datasets or third party data, please ensure that the statement adheres to our policy

All experimental data, analyzed data, and modeling simulations to support the findings of this study have been deposited at Dryad and are publicly available as of the date of publication.

Plasmid DNA sequences are available in the Supplementary Materials or Addgene. Plasmids not available through Addgene are available from the corresponding author upon request.

Policy information about studies with human participants or human data. See also policy information about sex, gender (identity/presentation),

All code for data analysis, modeling, and figure generation is publicly available on GitHub. Any additional information required to reanalyze the data reported in this paper is available from the corresponding author.

Research involving human participants, their data, or biological material

and sexual orientation and race, e	thnicity and racism.
Reporting on sex and gender	N/A
Reporting on race, ethnicity, or other socially relevant groupings	N/A
Population characteristics	N/A
Recruitment	N/A
Ethics oversight	N/A

Note that full information on the approval of the study protocol must also be provided in the manuscript.

Field-specific reporting

riease select the one below	w that is the best fit for your research	i. If you are not sure, read the appropriate sections before making your selection.		
X Life sciences	Behavioural & social sciences	Ecological, evolutionary & environmental sciences		
For a reference copy of the docum	nent with all sections, see <u>nature.com/documen</u>	uts/nr-reporting-summary-flat.pdf		
Life sciences study design				

Life sciences study design

All studies must disclose on these points even when the disclosure is negative.

All experiments shown in the main figures were conducted with at least 3 biological replicates, standard for similar studies in the field employing transient transfection, flow cytometry, and conversion experiments.

Data exclusions

Replicates of conversion that generated low cell counts at 5 dpi were excluded as related to issues with MEF batch preparation.

For each experiment, all data is representative of three independent, concordant experiments. All attempts at replication were successful.

Randomization

Randomization was not relevant in the study since the same cell line was grown up and divided among different wells prior to transfection.

Blinding

Groups were not blinded as sample preparation followed uniform protocols and all samples were analyzed in an automated fashion, with all results analyzed and displayed. For transfection studies, gating on a transfection marker was used to guarantee similar processing.

Reporting for specific materials, systems and methods

We require information from authors about some types of materials, experimental systems and methods used in many studies. Here, indicate whether each material, system or method listed is relevant to your study. If you are not sure if a list item applies to your research, read the appropriate section before selecting a response.

		į	
	2		1
	=		١
		١	
	ř		
	C		į

Materials & experime	ental systems Methods		
n/a Involved in the study	n/a Involved in the study		
Antibodies	ChIP-seq		
☐ ☐ Eukaryotic cell lines	Flow cytometry		
Palaeontology and a	archaeology MRI-based neuroimaging		
Animals and other o	organisms		
Clinical data			
Dual use research of	f concern		
1			
Antibodies			
Antibodies used			
Antibodies used Primary antibodies (Western Biot): Mouse anti p-actin (AH10D10) (1:50k dilution, Cell Signaling Technology, #3700, AB_2242 Mouse monoclonal ANTI-FLAG® M2 (1:20k dilution, Sigma-Aldrich, #F1804, RRID:AB_262044).			
	Secondary antibodies (Western Blot): Goat anti-mouse IgG H&L (HRP) (1:50k dilution, Abcam, ab205719, RRID:AB 2755049); Goat		
	anti-rabbit IgG H&L (HRP) (1:50k dilution, Abcam, ab6721, RRID:AB_955447).		
	Primary antibody (Flow): Mouse monoclonal ANTI-FLAG® M2 (1:400 dilution, Sigma-Aldrich, #F3165, RRID:AB 259529)		
	Secondary antibody (Flow): Goat anti-Mouse IgG (H+L) Cross-Adsorbed Secondary Antibody, Alexa Fluor™ 555 (1:400 dilution, Thermo Fisher Scientific, #A-21422, RRID:AB_2535844).		
	All information regarding the antibodies used is also available in the methods under "Immunofluorescent staining for flow" and		
	"Western Blot" subsections.		
Validation	Validation reported by vendor. Primary antibodies were commercially sourced and validated by their respective suppliers (Cell		
	Signaling Technologies, Sigma-Aldrich).		
muliaminatia aali liia			
Eukaryotic cell line			
Policy information about <u>ce</u>	ell lines and Sex and Gender in Research		
Cell line source(s) Human: HEK293T ATCC Cat#CRL-3216; Human: Plat-E Retroviral Packaging Cell Line Cell Biolabs, Inc. Cat#RV-101; Hi iPSC Line (Episomal, HFF), ALSTEM, Cat# iPS11; Mouse: B6.Cg-Tg(Hlxb9-GFP)1Tmj/J The Jackson Laboratory Cat#005 RRID:IMSR_JAX:005029 (Sex was not tested for, primary mouse embryonic fibroblasts isolated for this study were isofrom embryos of both sex).			
Authentication			
Addictitication	C57BL/6 mice were mated with mice bearing the Hb9::GFP reporter (B6.Cg-Tg(Hlxb9-GFP)1Tmj/J). Mouse embryonic fibroblasts with (for conversion experiments) or without Hb9::GFP reporter (for non-conversion experiments) were isolated at E12.5-E14.5 under a dissection microscope. Embryos are checked for Hb9::GFP reporter and sorted into non-transgenic and Hb9::GFP+ by illuminating spinal tissue with a blue laser to identify the presence of Hb9::GFP+ cells.		
	Commercial cell lines authenticated via source (HEK293T, iPS11, Plat-E), and did not undergo further validation in our lab.		
Mycoplasma contaminati	Cell lines were routine surveyed for mycoplasma to potential elminate contamination in samples.		
Commonly misidentified lines (See ICLAC register) None.			
Animals and othe	r research organisms		
Policy information about <u>st</u> <u>Research</u>	udies involving animals; ARRIVE guidelines recommended for reporting animal research, and Sex and Gender in		
Laboratory animals	Mice used were C57BL/6J The Jackson Laboratory Cat#000664 RRID: IMSR_JAX:000664, and B6.Cg-Tg(Hlxb9-GFP)1Tmj/J The Jackson Laboratory Cat#005029, RRID:IMSR_JAX:005029. C57BL/6 mice were mated with mice bearing the Hb9::GFP reporter (B6.Cg-Tg(Hlxb9-GFP)1Tmj/J). Male and female mice used for timed matings were >8 weeks old and pregnant females were taken for embryo isolation at day E14.5. Mice were housed in a 12-h light/ 12-h dark cycle with ambient temperature and humidity with access to food and water. Mice are housed in static microisolator caging with hardwood chip and a nestlet. Single housed animals also receive Enviro-Dri shredded paper nesting material and plastic houses. Cages are changed at least once weekly and spot checked daily.		
Wild animals	This study did not involve wild animals.		

Reporting on sex	Mouse embryonic fibroblasts were isolated from pregnant female mice. Isolated embryos were of both sexes.
Field-collected samples	This study did not involve samples collected from the field.
Ethics oversight	All mouse studies were approved and performed in compliance with the regulations of the Institutional Animal Care and Use Committee (IACUC) for Massachusetts Institute of Technology and The Whitehead Institute under protocol 2305000528.

Note that full information on the approval of the study protocol must also be provided in the manuscript.

ט	ı	n	+0
	ıa		LS

Seed stocks	N/A
Novel plant genotypes	N/A
Authentication	N/A

Flow Cytometry

Plots

Confirm that:

 \nearrow The axis labels state the marker and fluorochrome used (e.g. CD4-FITC).

The axis scales are clearly visible. Include numbers along axes only for bottom left plot of group (a 'group' is an analysis of identical markers).

All plots are contour plots with outliers or pseudocolor plots.

 ${\color{red} igwedge}$ A numerical value for number of cells or percentage (with statistics) is provided.

Methodology

Sample preparation

Bioreplicates represent separate transfection experiments.

To detach HEK293T or MEF cells from wells in preparation for flow cytometry, Trypsin (Genesee Scientific 25-510) diluted in PBS was added to the well. After 8 minutes, DMEM (Genesee Scientific 25-500) + 10% FBS (Genesee Scientific 25-514H) was added on top. iPS11 cells were dissociated into single cells using Gentle Cell Dissociation Reagent (STEMCELL Technologies, 100-1077). For conversion quantification of MEFs to iMNs at 14 dpi, cells were dissociated using DNase/Papain dissociation system

For 96-well plates, cells were centrifuged in plates at $1000 \times g$ for 10 minutes. For 12-well plates or 6-well plates, cells were centrifuged in tubes at $400 \times g$ for 5 minutes. As described, cells underwent HCR Flow FISH (RNA FISH) or immunofluorescent staining. For flow, cells were resuspended in $1 \times PBS$. For 96-well experiments, cells were transferred to a round bottom plate for flow cytometry. Detailed methods are included in the main text.

Instrument

Attune NxT Acoustic Focusing Cytometer

Software

Live cells were gated based on FSC-A and SSC-A using FlowJo v10. Subsequently, single cells were gated via SSC-H and SSC-A. Single cells were then exported all plots and statistics were generated from pandas, matplotlib, statannot, pandas, and seaborn packages in Python.

Cell population abundance

For analysis, single live cells were gated based on FSC, SSC, and transfection markers unless otherwise described.

Gating strategy

Representative gates are included in the supplement Figures S1 and S2 with details on gating rationale.

Tick this box to confirm that a figure exemplifying the gating strategy is provided in the Supplementary Information.

